

Conference paper

Galina F. Makhaeva, Elena F. Shevtsova, Alexey Y. Aksinenko, Nadezhda V. Kovaleva, Natalia P. Boltneva, Sofya V. Lushchekina, Elena V. Rudakova, Elena A. Pushkareva, Tatyana P. Serkova, Lyudmila G. Dubova, Pavel N. Shevtsov, Vladimir B. Sokolov^a, Eugene V. Radchenko, Vladimir A. Palyulin, Sergey O. Bachurin and Rudy J. Richardson*

Bis- γ -carbolines as new potential multitarget agents for Alzheimer's disease

<https://doi.org/10.1515/pac-2019-1206>

Abstract: A new series of homobivalent Dimebon analogs, bis- γ -carbolines with alkylene, phenylenedialkylene, and triazole-containing spacers, was synthesized. Doubling the γ -carboline pharmacophore increased inhibitory potency against acetylcholinesterase (AChE) compared with Dimebon, while keeping Dimebon's anti-butyrylcholinesterase activity; therefore, leading to inversion of selectivity. Molecular docking revealed the reasons for the increased anti-AChE activity and ability to block AChE-induced aggregation of β -amyloid for bis- γ -carbolines, which became double-site inhibitors of AChE. Conjugates with ditriazole-containing spacers were the most active antioxidants in both the ABTS-test and prevention of lipid peroxidation in brain homogenates without inhibiting the mitochondrial permeability transition (MPT). Conjugates with alkylene (**4a–d**), phenylenedialkylene (**4e**), and monotriazole (**8**) spacers were less active as antioxidants but prevented induction of the MPT and increased the calcium retention capacity of mitochondria. Lead compound **4e** showed neuroprotective potential in a cellular calcium overload model of neurodegeneration. Computational studies showed that all the bis- γ -carbolines were expected to have high values for intestinal absorption and very good blood-brain barrier permeability along with good drug-likeness. Overall, the results showed that new homobivalent Dimebon analogs exhibit an expanded spectrum of biological activity and improved pharmacological properties, making them promising candidates for further research and optimization as multitarget agents for Alzheimer's disease treatment.

Keywords: acetylcholinesterase; Alzheimer's disease; antioxidants; bis- γ -carbolines; butyrylcholinesterase; calcium retention capacity; Mendeleev-21; MPT; multitarget agents; neuroprotection; pharmacological profile.

Article note: A collection of invited papers based on presentations at 21st Mendeleev Congress on General and Applied Chemistry (Mendeleev-21), held in Saint Petersburg, Russian Federation, 9–13 September 2019.

^aDeceased

*Corresponding author: Dr. Rudy J. Richardson, Departments of Environmental Health Sciences and Neurology, University of Michigan, Ann Arbor, Michigan 48109, USA; Center for Computational Medicine and Bioinformatics, University of Michigan, Ann Arbor, Michigan 48109, USA; and Molecular Simulations Laboratory, M6065 SPH-II 2029, University of Michigan, 1415 Washington Heights, Ann Arbor, Michigan 48109-2029, USA, Phone: +1-734-936-0769, Fax: +1-734-763-8095, E-mail: rjrich@umich.edu

Galina F. Makhaeva, Elena F. Shevtsova, Alexey Y. Aksinenko, Nadezhda V. Kovaleva, Natalia P. Boltneva, Elena V. Rudakova, Elena A. Pushkareva, Tatyana P. Serkova, Lyudmila G. Dubova, Pavel N. Shevtsov, Vladimir B. Sokolov and Sergey O. Bachurin: Institute of Physiologically Active Compounds Russian Academy of Sciences, Chernogolovka 142432, Russia

Sofya V. Lushchekina: Institute of Physiologically Active Compounds Russian Academy of Sciences, Chernogolovka 142432, Russia; and Emanuel Institute of Biochemical Physics of Russian Academy of Sciences, Moscow 119334, Russia

Eugene V. Radchenko and Vladimir A. Palyulin: Institute of Physiologically Active Compounds Russian Academy of Sciences, Chernogolovka 142432, Russia; and Department of Chemistry, Lomonosov Moscow State University, Moscow 119991, Russia

Introduction

Alzheimer's disease (AD) is a progressive and irreversible neurodegenerative disorder, which is one of the most common form of dementia in the elderly [1]. It is a multifactorial disease with a vicious circle of complex pathogenic processes. AD is one of the greatest challenges of the current search for new drugs [2–4]. Accordingly, clinically effective drugs for the treatment of AD have not yet emerged. This lack of progress is likely due not only to the complex multifactorial nature of the disease but also to the late manifestation of symptoms. These factors result in arriving at a diagnosis of AD after the processes of neurodegeneration have already developed in the brain.

Although the etiology of AD is not completely known, current hypotheses of AD pathogenesis are based on aberrant protein deposition (β -amyloid and tau protein), oxidative stress, mitochondrial dysfunction, and dysfunction of cholinergic and glutamatergic systems.

Acetylcholinesterase (AChE, EC 3.1.1.7) is one of the major targets in the current therapy of AD. Consequently, cholinergic drugs such as rivastigmine, galantamine and donepezil, along with the NMDA receptor antagonist memantine, constitute the main pharmacotherapeutic group used for the symptomatic treatment of the disease. For improved efficacy of therapeutic intervention by cholinesterase inhibitors, attention is currently focused on an additional target, butyrylcholinesterase (BChE, EC 3.1.1.8). In the healthy brain, acetylcholine is dominantly hydrolyzed by AChE, whereas in AD, the AChE level in the brain decreases progressively, but BChE activity elevates [5, 6]. While treatment with selective AChE inhibitors is effective in the beginning stages of AD, their effectiveness decreases with progression of the disease, which may be due in part to lower AChE activity. Thus, BChE is a proposed drug target for treatment of the advanced stages of AD. It is believed that compounds inhibiting both cholinesterases increase the efficiency of treatment [6, 7].

The formation of β -amyloid ($A\beta$) deposits is typical of the early pathogenesis in AD. The discovery of additional functional features of AChE, in particular, the ability of the peripheral anionic site (PAS) to induce β -amyloid aggregation [8–11] has been revealed. It was found that PAS ligands, such as propidium, blocked AChE-induced $A\beta$ aggregation by physically hampering $A\beta$ binding to the enzyme surface [10, 12, 13]. Moreover, dual-binding molecules that interact with both the catalytic active site (CAS) and the PAS of AChE can inhibit AChE activity and block its amyloidogenic properties. Such compounds could simultaneously improve cognitive function and exert disease-modifying properties [14–18]. BChE is also involved in the formation and/or maturation of $A\beta$ plaques and thereby contributes to the pathogenesis of AD [19–21]. Therefore, inhibitors of both cholinesterases are of interest from the point of view of anti-amyloid strategy.

A highly desirable property of potential drugs for treatment of neurodegenerative diseases is neuroprotection. Prospective targets for this type of activity are deleterious processes affecting mitochondria – in particular, oxidative stress and the mitochondrial permeability transition (MPT).

Oxidative stress is characterized by an imbalance between the formation of reactive oxygen species (ROS) and their inactivation through various components of the antioxidant system. The resultant oxidative impairments of membrane lipids and proteins constitute a vicious cycle of self-propagating injury in the development of neurodegenerative diseases [22, 23]. It is believed that oxidative stress is associated with such pathological processes as the generation and accumulation of β -amyloid, disturbance of metal ion homeostasis, and mitochondrial dysfunction and increased vulnerability to MPT induction [24, 25].

The MPT is associated with the opening of a non-specific pore in the mitochondrial inner membrane, and this phenomenon plays a central role in cell death. Moreover, susceptibility to the MPT is enhanced with aging and age-related degenerative diseases. Mitochondria play important roles in the production of amyloid peptides and generation of ROS, and simultaneously mitochondria are the targets of the toxic actions of these species [26]. Thus, the search for effective mitoprotective agents has great potential for uncovering compounds that could be useful in AD therapeutics [27, 28].

Taking into account the multiplicity of biological targets and pathways involved in the pathogenesis and progression of AD, creating multifunctional molecules or Multi-Target-Directed-Ligands that have a synergistic effect on a number of biological targets responsible for the pathogenesis of the disease is a promising strategy

[3, 4, 29–37]. The multitarget approach is currently one of most fruitful drug discovery areas, particularly in developing medicines against major complex diseases [38–41].

Multi-target compounds are rationally designed, typically by combining two distinct pharmacophores into a single chemical entity, starting from compounds with the desired activity toward the targets of interest. In addition, two identical pharmacophores can be combined through a spacer, thereby producing homodimers or so-called homobivalent ligands [42–44]. This doubling of pharmacophores may extend the range of pharmacological activity beyond that of the parent molecule by enhancing the properties of the original compound or giving rise to new biological activities [30, 42–51]. To source the components of such conjugates, known drugs that have already been released on the pharmaceutical market or agents that have shown efficacy in preclinical trials are often used.

To create new homobivalent compounds, we used as a pharmacophore the tetrahydro- γ -carboline fragment of the drug Dimebon. It is a multifunctional drug that has the ability to protect neurons from death; in particular, due to its effect on mitochondria. It also reduces the development of proteinopathies and stimulates autophagy, combining these properties with its effect on a number of neurotransmitter targets, including inhibition of AChE ($IC_{50}=42\text{ }\mu\text{M}$) and BChE ($IC_{50}=7.9\text{ }\mu\text{M}$) [52]. Neuroprotective and cognition-stimulating effects of Dimebon have been well studied, and its efficacy has been shown in numerous preclinical studies as well as during the second stage of clinical trials [53–55]. Quite successful attempts have already been made to create homobivalent compounds based on this interesting and promising molecule, which have shown a significant increase in anti-AChE activity and increased inhibition of A β self-aggregation while maintaining the level of NMDA receptor blockade [30, 43, 51]. Our study in this direction began with the creation of homodimers of the γ -carboline fragment of Dimebon combined with a bis-triazole spacer, recently published as a short communication [56].

We believe that new multi-targeted molecules, in order to be effective anti-AD medicines, should combine compensatory cognition-stimulating properties, neuroprotective potential, and the so-called disease-modifying effect; in particular, disease associated with the aggregation of β -amyloid.

In this context, we present here the synthesis and comparative investigation of the pharmacological profiles of new homobivalent ligands – bis- γ -carbolines combined with four different types of spacers: alkylene, phenylenedialkylene, mono- and ditriazole (Fig. 1) as potential multifunctional agents for the treatment of AD. This work included studying the esterase profile of the conjugates – their inhibitory activity against cholinesterases and a structurally related enzyme, carboxylesterase (CES, EC 3.1.1.1), with quantum mechanics (QM)-assisted molecular docking. In addition, we measured propidium displacement from the AChE PAS as an assessment of their potential to block AChE-induced aggregation of A β , along with

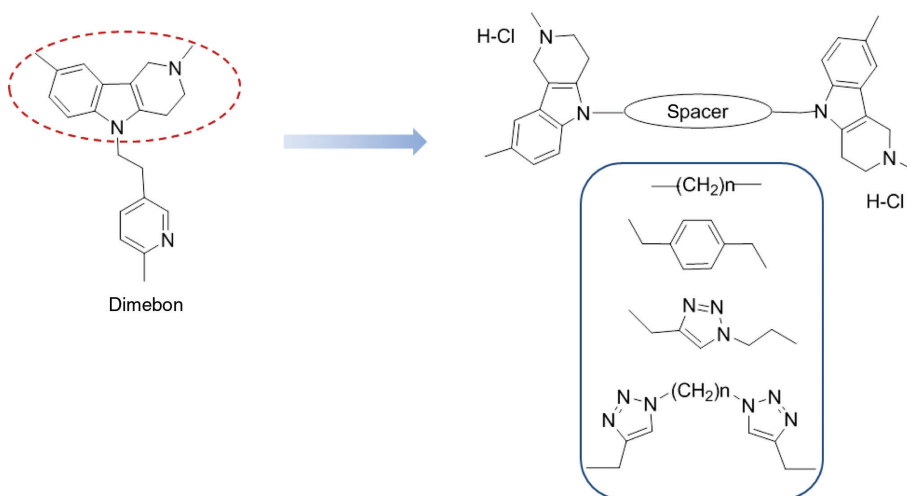


Fig. 1: Dimebon and its homobivalent analogs – bis- γ -carbolines linked through alkylene, phenylenedialkylene, and mono- and ditriazole spacers.

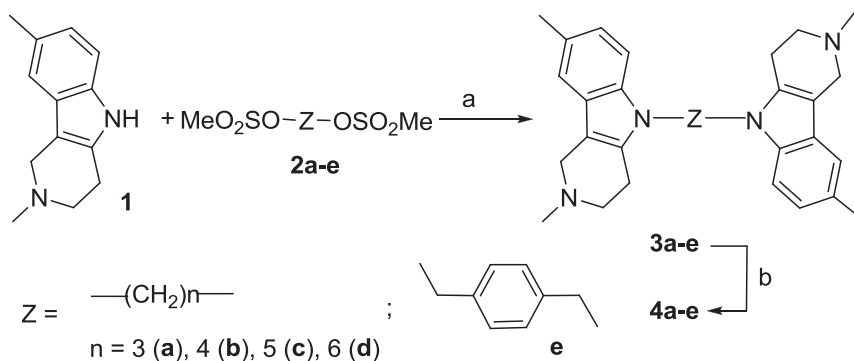
antioxidant activity, MPT inhibition, and the calcium retention capacity of brain mitochondria. Confirmation of neuroprotection was assessed using a calcium overload model of neurodegeneration. To assess potential pharmacokinetic properties of the new structures, we determined ADMET profiles computationally.

Results and discussion

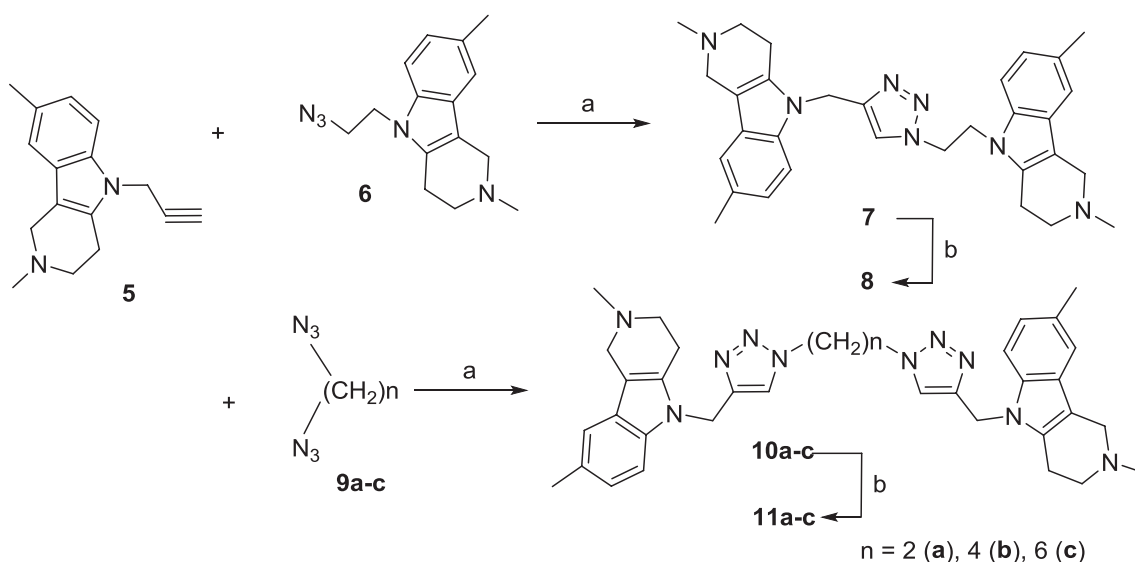
Synthesis

Bis-γ-carbolines **4a–e** were obtained by the reaction of tetrahydro-γ-carboline **1** with alkyldimethanesulfonates **2a–e** in the presence of 0.5 equivalents of NaH, as previously described [57], with subsequent conversion of isolated bis-γ-carbolines **3a–e** into the corresponding hydrochlorides **4a–e** (Scheme 1).

Synthesis of bis-γ-carbolines **7** and **10a–c** was performed by reaction of N-propargyltetrahydro-γ-carboline **5** with N-azidoethyltetrahydro-γ-carboline **6** and terminal diazidoalkanes **9a–c**, respectively, in the presence of catalytic amounts of Cu(I) (Scheme 2). The reaction mixture was stirred for 3–4 h at 40 °C. The target bis-γ-carbolines **7**, **10a–c** were isolated and purified by column chromatography in 78–81 % yields [58], and then were converted into the corresponding hydrochlorides **8**, **11a–c**.



Scheme 1: Synthesis of bis-γ-carbolines **3** and **4**. Reagents and conditions: (a) NaH, THF, r.t., 6 h; (b) HCl, acetone, r.t.



Scheme 2: Synthesis of bis-γ-carbolines **7**, **8**, **10**, **11**. Reagents and conditions: (a) CuSO₄, Na ascorbate, DCM, 40 °C, 4 h; (b) HCl, acetone, r.t.


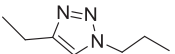
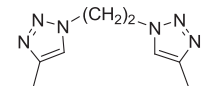
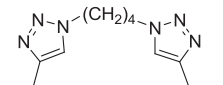
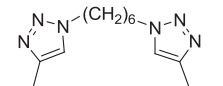
Study of the inhibitory activities of bis- γ -carbolines toward AChE, BChE and CES

We determined esterase profile of bis- γ -carbolines – their inhibitor activity toward two cholinesterases and CES, a structurally related enzyme. CES is a key enzyme of hydrolytic metabolism of many clinically used medicines containing ester, amide, and carbamate groups [59, 60]. The ability of anticholinesterase compounds used for the therapy of AD to inhibit CES may lead to undesirable drug-drug interactions [61]. A comparative assessment of the inhibitory activity of new compounds against several related serine esterases allows us to elucidate both their potential primary pharmacological effect and possible adverse effects [36, 62–66].

Results on the esterase profile of the synthesized bis- γ -carbolines are presented in Table 1. As can be seen, the bis- γ -carbolines practically do not inhibit CES, which is a desirable result. The inhibitory activity of the tested compounds against cholinesterases, AChE and BChE, was dependent upon the structure of the spacer.

As can be seen from Table 1, in the series of conjugates **4a–d**, a smooth increase in anti-AChE activity was obtained with an increase in the length of the alkylene spacer $-(CH_2)_n-$. An increase in the spacer length from $n=3$ (**4a**) to $n=6$ (**4d**) led to a 6-fold increase in anti-AChE activity. Bis- γ -carbolines with phenylenedialkylene **4e** and monotriazole **8** spacers exhibited almost the same moderate anti-AChE activity with an IC_{50} of about 10 μ M. In contrast, for symmetric bis- γ -carbolines **11a–c** with ditriazole spacers there was a sharp increase in

Table 1: Esterase profile of bis- γ -carbolines and their ability to displace propidium from the *Ee*AChE PAS.

Compound	Spacer	IC_{50} (μ M) \pm SEM or inhibition % at 20 μ M			Displacement of propidium from the <i>Ee</i> AChE PAS ^d by the compound at 20 μ M (%)
		AChE ^a	BChE ^b	CES ^c	
4a	$-(CH_2)_3-$	15.68 \pm 1.01	4.96 \pm 0.10	n.a.	14.4 \pm 1.2
4b	$-(CH_2)_4-$	12.31 \pm 1.86	7.62 \pm 0.26	17.9 \pm 1.6 %	15.9 \pm 1.4
4c	$-(CH_2)_5-$	5.37 \pm 0.08	6.56 \pm 0.58	12.2 \pm 0.5 %	17.9 \pm 1.5
4d	$-(CH_2)_6-$	2.74 \pm 0.26	3.38 \pm 0.16	16.2 \pm 0.4 %	19.4 \pm 1.5
4e		9.03 \pm 0.43	0.572 \pm 0.053	41.3 \pm 1.0 %	14.5 \pm 1.3
8		10.5 \pm 1.0	13.2 \pm 0.8	3.0 \pm 0.2 %	16.3 \pm 1.4
11a		9.2 \pm 0.2 % ^e	38.3 \pm 2.6 ^e	3.2 \pm 0.8 % ^e	n.d. ^e
11b		22.4 \pm 2.2 ^e	41.9 \pm 1.2 ^e	3.7 \pm 1.0 % ^e	13.1 \pm 1.1 ^e
11c		0.772 \pm 0.005 ^e	4.75 \pm 0.06 ^e	7.4 \pm 0.4 % ^e	23.7 \pm 1.8 ^e
Dimebon		36.3 \pm 3.59	5.76 \pm 0.51	n.a.	4.0 \pm 0.5
Donepezil		0.0400 \pm 0.0037	19.2 \pm 2.97	>100	10.5 \pm 0.8
Galantamine		1.02 \pm 0.06	15.8 \pm 0.90	>100	n.d.

^aHuman erythrocyte AChE.

^bEquine serum BChE.

^cPorcine liver CES.

^d*Electric eel* AChE peripheral anionic site.

n.a., Not active.

n.d., Not determined.

^e[56].

inhibitor potency with increasing spacer length: from very weak ($9.2 \pm 0.2\%$ at $20 \mu\text{M}$) for conjugate **11a** ($n=2$) to a rather strong submicromolar value ($\text{IC}_{50} = 0.772 \pm 0.005 \mu\text{M}$) for **11c** ($n=6$).

Most bis- γ -carbolines, with the exception of compound **11a**, inhibited AChE more efficiently than Dimebon; i.e., the duplication of the molecule increased inhibitory potency against AChE. The most active conjugate **11c** was 47-fold more potent than the parent compound and more active than the marketed drug galantamine ($\text{IC}_{50} = 1.02 \pm 0.06 \mu\text{M}$).

As for the inhibition of BChE, doubling the γ -carboline pharmacophore using an alkylene spacer (**4a–d**) and a long ditriazole spacer (**11c**), maintained the high micromolar anti-BChE activity of Dimebon, whereas conjugates with short ditriazole spacers (**11a,b**) and a monotriazole spacer (**8**) were less active.

A particularly noteworthy finding was the sharp increase in anti-BChE activity (more than 20 times) when replacing the monotriazole spacer (**8**) with phenylenedialkylene (**4e**). Conjugate **4e** was the most potent BChE inhibitor among the studied bis- γ -carbolines, while compounds **8** and **4e** possessed equal anti-AChE activity (Table 1).

In addition, it should be noted that Dimebon is characterized by preferential inhibition of BChE, while bis- γ -carbolines with a long spacer (alkylene **4d** or bistriazolalkylene **11c**) were more effective toward AChE. A similar effect of inversion of selectivity was seen for other described homobivalent bis- γ -carbolines [43, 51].

Kinetic measurements

All of the studied bis- γ -carbolines showed a mixed-type inhibition of cholinesterases. The mechanism of AChE and BChE inhibition by the conjugates is demonstrated for compound **11c** as an example. Graphical analysis using double reciprocal Lineweaver–Burk plots is shown in Fig. 2. The plots demonstrate that the binding of conjugate **11c** to either AChE or BChE resulted in changes in V_{\max} and K_m . This is consistent with a mixed-type inhibition. The values of AChE and BChE inhibition constants (K_i =competitive component and αK_i =non-competitive component) are shown in Table 2.

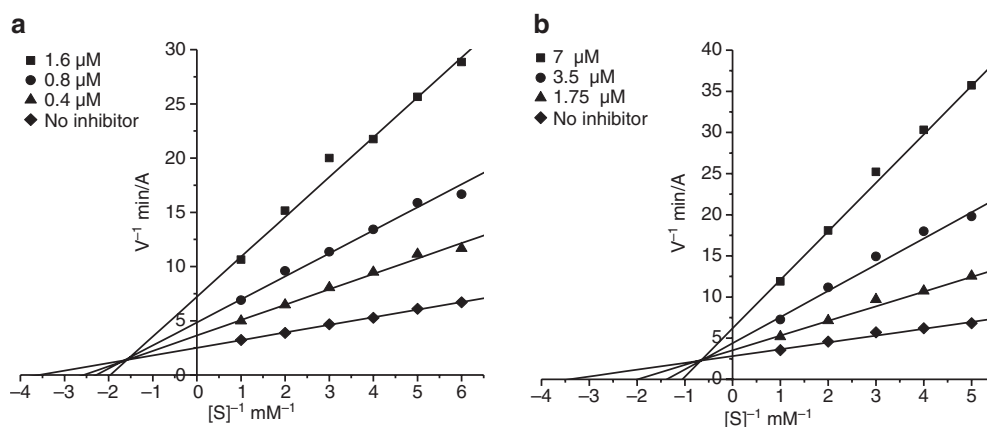


Fig. 2: Lineweaver-Burk double-reciprocal plots of steady state inhibition of AChE (a) and BChE (b) by compound **11c**. Each plot indicates mixed-type inhibition.

Displacement of propidium iodide from the peripheral anionic site of *Ee*AChE

A fluorescence assay used to evaluate competitive propidium displacement from the PAS of AChE is commonly used as a primary screening method for AChE pro-aggregation activity inhibitors [15]. Propidium is a selective ligand for the PAS of AChE responsible for A β binding [8, 12]. It exhibits a fluorescence increase upon binding

Table 2: The inhibition constants of AChE and BChE by some bis- γ -carbolines.^a

Compound	AChE		BChE	
	K_i (μM)	αK_i (μM)	K_i (μM)	αK_i (μM)
4d	0.93 ± 0.08	1.66 ± 0.05	0.73 ± 0.02	2.33 ± 0.21
8	8.64 ± 0.54	16.0 ± 0.8	5.36 ± 0.35	22.7 ± 1.8
11b	7.18 ± 0.06	11.4 ± 0.4	21.2 ± 2.0	89.0 ± 8.6
11c	0.384 ± 0.037	0.810 ± 0.080	0.905 ± 0.069	5.66 ± 0.02

^aValues for K_i (competitive inhibition constant) and αK_i (non-competitive inhibition constant) were determined from analyses of slopes of $1/V$ vs. $1/S$ at various inhibitor concentrations. Values (means \pm SEM) are from at least three separate experiments.

to AChE. The fluorescence intensity of propidium iodide bound with AChE increases several times [67]. A decrease of fluorescence intensity of the bound propidium in the presence of the test compounds shows their ability to bind to the PAS of AChE, thereby displacing propidium, which predicts that the compounds would block the AChE-mediated aggregation of A β [15]. Donepezil was used as the reference compound, as it is in clinical use, and it is a mixed-type AChE inhibitor for which the ability to block AChE-PAS-induced A β aggregation has been demonstrated [10]. The results are presented in Table 1.

The results show that all bis- γ -carbolines displaced propidium from the PAS of AChE more effectively than the reference compound donepezil (i.e. $>10.5 \pm 0.8\%$) and substantially exceeded the displacement achieved by Dimebon (i.e. $>4.0 \pm 0.5\%$). Elongation of the alkylene spacer from $n=3$ (**4a**) to $n=6$ (**4d**) in conjugates **4a–d** led only to a small increase in the degree of propidium displacement ($14.4 \pm 1.2\%$ – $19.4 \pm 1.5\%$). A significant effect was not observed when a phenylene **4e** ($14.5 \pm 1.3\%$) or triazole **8** ($16.3 \pm 1.4\%$) fragment was introduced into the spacer. However, for symmetrical bis- γ -carbolines with two triazoles in the spacer, an increase in the length of the intertriazole alkylene fragment from $n=4$ (**11b**) to $n=6$ (**11c**) led to an almost twofold increase in the degree of propidium displacement (13.1 ± 1.1 vs. $23.7 \pm 1.8\%$, respectively).

Molecular modeling

Molecular docking of the bis- γ -carbolines to AChE and BChE was performed to gain insight into the modes of ligand-protein binding. Results of molecular docking of these homobivalent ligands to AChE PDB ID 4EY7 (Fig. 3a–c) showed that one of γ -carboline fragments binds to the active site of AChE at the bottom of the gorge, mostly due to π - π -stacking interactions with Trp86, regardless of the spacer type. There was some difference in orientation of the γ -carboline ring of conjugates **4a,d** (Fig. 3a), **4e**, **8** (Fig. 3b) compared with **11a–c** (Fig. 3c) allowing the former to have ionic interactions with the Glu202 side chain. Comparison of molecular docking results obtained for different AChE X-ray structures showed sensitivity of the position of the compounds to conformation of the residues inside the gorge as was discussed in detail in an earlier report [68].

With increasing length of the spacer, the position of the second γ -carboline ring in the PAS became more favorable: π - π -stacking and π -cationic interactions with Trp286 were obtained, and this tendency was observed for conjugates with alkylene as well as ditriazole spacers. In the latter case, this effect was more pronounced due to a more rigid structure. One of triazole rings of the spacers in conjugates **11a–c**, located below the bottleneck, was able to form weak hydrogen bonding interactions, e.g. with Tyr124 (Fig. 3c). For other compounds, specific interactions between the spacer elements and the gorge residues were not observed. For conjugate **11c** with the longest ditriazole spacer, ionic interactions with Glu292 were formed (Fig. 3c). This corresponds well with the experimentally observed sharp increase in anti-AChE activity and propidium displacement. No significant differences in AChE binding were found for compounds with phenylenedialkylene (**4e**) and monotriazole (**8**) spacers (Fig. 3b), which agrees with their close inhibitor activity.

In contrast, for inhibition of BChE (Fig. 3d–f), a difference in the positions of compounds **8** and **4e** with phenylenedialkylene and monotriazole spacers was observed. Due to a more rigid spacer, compound **4e** did not bend inside the wide BChE gorge. Instead, it was found in an elongated conformation and formed

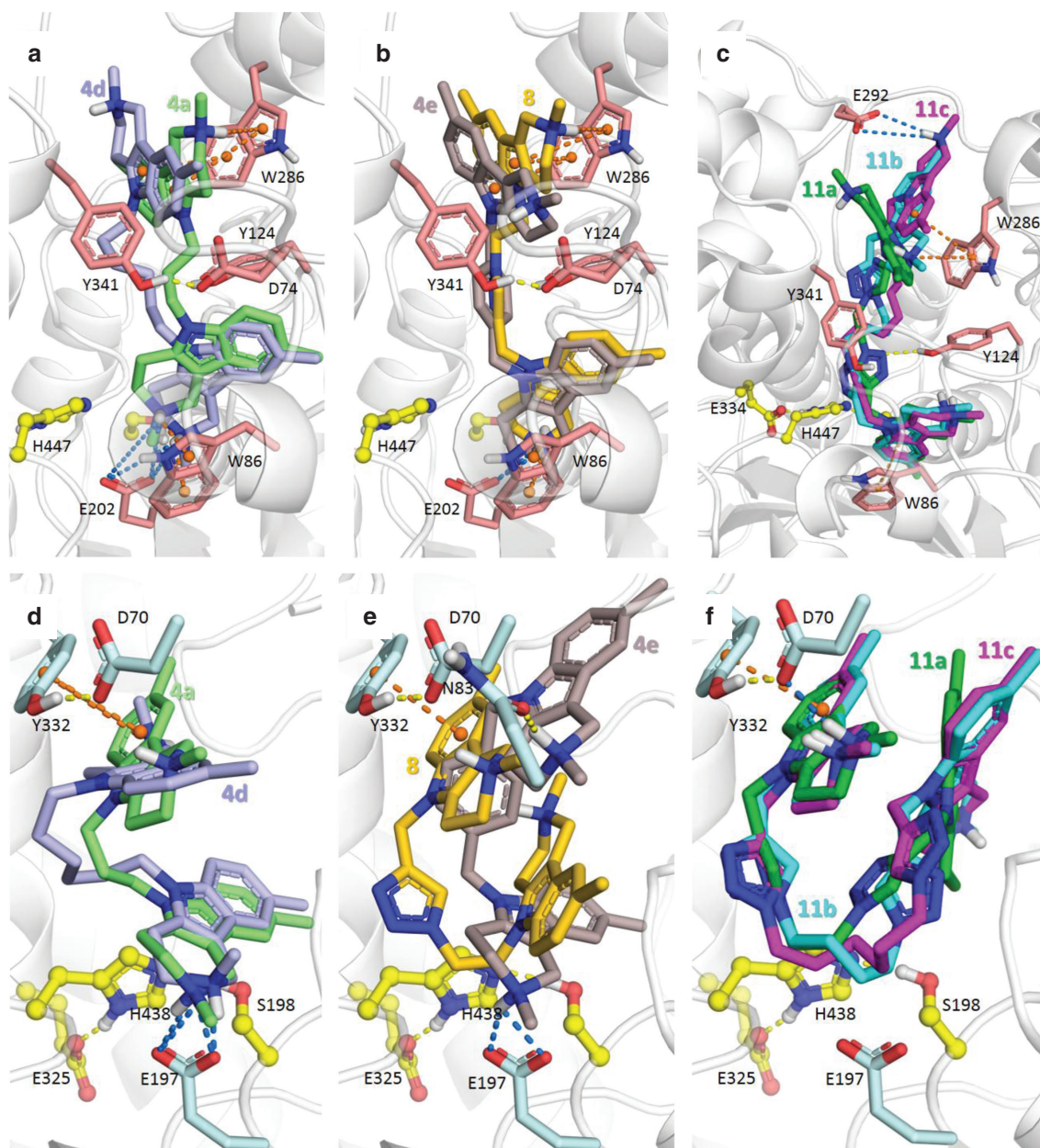


Fig. 3: Results of molecular docking of bis- γ -carbolines into (a–c) human AChE (carbon atoms of side chains are shown in pink) and (d–f) human BChE (carbon atoms of side chains are shown in light blue). Carbon atoms of the catalytic triads of each enzyme are shown in yellow. Orange dashed lines show π - π -stacking and π -cationic interactions, blue dashed lines show ionic interactions, and yellow dashed lines show hydrogen bonds. Carbon atoms of compound **4a** are shown in light-green, **4d** – light-blue (a, d); **4e** – brown, **8** – gold (B,E); **11a** – green, **11b** – cyan, **11c** – magenta (e, f).

specific interactions: an ionic interaction with Glu197 in the active site and a hydrogen bond with Asn83 in the PAS (Fig. 3e). Conjugates with an alkylene spacer **4a–d** were also able to form an ion pair between the nitrogen atom of the γ -carboline ring and Glu197, but the second γ -carboline ring formed π - π stacking interactions with the Tyr332 ring (Fig. 3d). In spite of different lengths of the spacer, the positions of **4a** and **4d** were very similar (Fig. 3d). For compounds **11a–c** with a ditriazole spacer, the spacer length also did not affect the position of the compound bound in the BChE gorge. The BChE gorge is wide enough to accommodate compounds with lengthy and flexible spacers in bent conformations [36]. One of the γ -carboline fragments of compounds **11a–c** forms π - π interactions and salt bridges with Tyr332 and Asp70, respectively (Fig. 3f). The second γ -carboline fragment is located in a very similar way regardless of different

linker lengths, though it is not engaged in specific interactions, mostly due to its geometrical fit to the gorge. Thus, the length of the spacer does not affect significantly the location of γ -carboline rings and binding affinity to BChE.

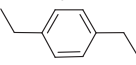
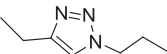
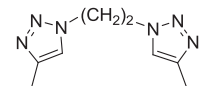
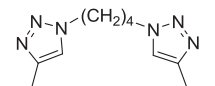
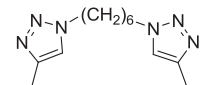
Thus, the results of molecular docking reveal the reasons for the increased anti-AChE activity of the homodimers of γ -carboline that became double-site inhibitors of AChE, their ability to block AChE-induced aggregation of A β , and the observed structure-activity relationships.

Antioxidant activity of bis- γ -carbolines

Primary antioxidant activity of the compounds was determined spectrophotometrically by the ABTS assay [69], in which a decrease in absorbance of the cation-radical ABTS⁺ (2,2'-azinobis-(3-ethylbenzothiazoline-6-sulfonic acid)) is measured at $\lambda = 734$ nm after its interaction with an antioxidant compound as previously described in detail [70]. Trolox was used as a reference antioxidant. The results were expressed as TEAC values (Trolox equivalent antioxidant capacity) calculated by dividing the slope of ABTS⁺ concentration decrease vs. the tested antioxidant concentration by the slope for the Trolox plot.

The results of the ABTS test (Table 3) show that conjugates **4a–d** linked through an alkylene spacer exhibited rather weak antiradical activity with a tendency to increase slightly with increasing spacer length

Table 3: The radical-scavenging activity of bis- γ -carbolines in the ABTS test and their ability to inhibit lipid peroxidation (LP) in rat brain homogenates.

Compound	Spacer	Antiradical activity, ABTS test		Inhibition of LP in rat brain homogenates	
		TEAC ^a	IC ₅₀ ^a , μ M	Fe ²⁺ -induced, IC ₅₀ , μ M	Residual tBHP-induced LP, % of control at 30 μ M
4a	–(CH ₂) ₃ –	0.03 \pm 0.001	n.d.	25.9 \pm 8.4	97 \pm 8
4b	–(CH ₂) ₄ –	0.065 \pm 0.003	n.d.	\geq 30	92 \pm 9
4c	–(CH ₂) ₅ –	0.1 \pm 0.006	n.d.	9.9 \pm 2.0	89 \pm 10
4d	–(CH ₂) ₆ –	0.086 \pm 0.007	n.d.	14.3 \pm 4.8	90 \pm 14
4e		0.047 \pm 0.002	n.d.	23.1 \pm 11.1	90 \pm 14
8		0.25 \pm 0.013	96.3 \pm 2.8	13.0 \pm 3.1	96 \pm 3
11a		0.91 \pm 0.05 ^b	20.3 \pm 2.2	3.0 \pm 0.5 ^b	82 \pm 3
11b		0.77 \pm 0.04 ^b	26.5 \pm 1.3	3.1 \pm 0.6 ^b	78 \pm 5
11c		0.27 \pm 0.015 ^b	104.3 \pm 3.2	2.8 \pm 0.6 ^b	94 \pm 4
Dimebon		0.004 \pm 0.001	n.d.	>100	103 \pm 7
Trolox		1.0	20.4 \pm 1.2	31 \pm 6	–

n.d., Not determined.

^aTEAC values (Trolox equivalent antioxidant capacity) calculated by dividing the slope of ABTS⁺ concentration decrease vs. the tested antioxidant concentration by the slope for the Trolox plot.

IC₅₀ values = concentration of compound (μ M) required to reduce concentration of ABTS⁺ by 50 %.

Results were obtained from 3 replicates of each sample and 3 independent experiments.

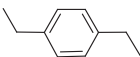
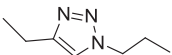
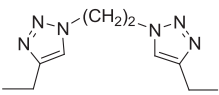
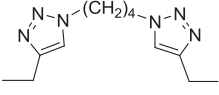
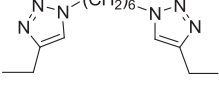
^b[56].

(TEAC=0.03–0.1). Compound (**4e**) with a phenylenedialkylene spacer also demonstrated low antiradical activity. On the contrary, symmetric homodimers **11a,b** with ditriazole spacers possessed radical-scavenging activity comparable to that of the standard antioxidant Trolox. Moreover, the ABTS-scavenging activity of the compounds depended on the structure and length of the spacer: conjugate **8** with a monotriazole spacer possessed moderate antiradical activity (TEAC=0.25). As for conjugates with ditriazole spacers, compounds with the shorter spacer **11a** ($n=2$) and **11b** ($n=4$) scavenged free radicals with high efficiency – at the level of the standard antioxidant Trolox, while elongation of the intertriazole alkylene chain to $n=6$ (compound **11c**) somewhat reduced antiradical activity.

These results suggest a significant role of triazole spacers for the radical-scavenging activity of bis- γ -carbolines in the realization of their antioxidant potency.

To obtain information about the antioxidant activity in a biological system, we studied the ability of the bis- γ -carbolines to suppress lipid peroxidation (LP) in the crude membrane fraction from rat brain homogenates. In the biological *in vitro* system all the studied bis- γ -carbolines were able to inhibit Fe²⁺-induced LP significantly more effectively than Dimebon (Table 3), but were almost ineffective against tBHP-induced LP. Compounds with ditriazole-containing spacers **11a–c**, as in the ABTS test, showed the highest activity as antioxidants. These results allowed us to assume a significant role of the radical-scavenging activity of

Table 4: Effects of bis- γ -carbolines on mitochondrial potential and calcium-induced MPT.

Compound	Spacer	Depolarization of mitochondria after 10 min incubation with 30 μ M of compounds, %	V_{\max} of Ca ²⁺ -induced swelling of mitochondria with 30 μ M of compounds, dA_{620}/dt , %		Inhibition of Ca ²⁺ -induced swelling of mitochondria, IC ₅₀ , μ M
			10 μ M	30 μ M	
4a	–(CH ₂) ₃ –	n.a.	83.1 \pm 6.8	33.4 \pm 5.9	24.3 \pm 7.6
4b	–(CH ₂) ₄ –	3.6 \pm 0.9	33.7 \pm 9.9	17.1 \pm 3	5.8 \pm 1.2
4c	–(CH ₂) ₅ –	5.3 \pm 2	71.2 \pm 2.2	48.4 \pm 8.9	23.5 \pm 8.1
4d	–(CH ₂) ₆ –	5.0 \pm 1.6	68.7 \pm 12.5	28.2 \pm 5.3	15.9 \pm 5.5
4e		7.1 \pm 2.4	18.2 \pm 4.4	– ^a	2.4 \pm 0.9
8		n.a.	52.4 \pm 9.9	24.4 \pm 1.9	8.9 \pm 2.2
11a		9.1 \pm 1.3	n.d.	133.6 \pm 9.8	n.d.
11b		8.5 \pm 1.3	n.d.	119.6 \pm 5.4	n.d.
11c		13.7 \pm 1.8	n.d.	107.9 \pm 4.8	n.d.
Dimebon		n.a.	70.3 \pm 14	49.5 \pm 10.3	37 \pm 17.5

^aDid not exceed the spontaneous swelling.

n.a., Not active.

n.d., Not determined.

triazole-bearing bis- γ -carboline in the realization of their antioxidant activity, except that we could not see a dependence of the degree of LP suppression on the length of the ditriazole spacer. At the same time, conjugates linked through alkylene and phenylenedialkylene spacers did not reveal significant radical scavenging activity, although they possessed antioxidant activity in the LP test.

Effect of bis- γ -carboline on the characteristics of mitochondria

As a primary screening, mitochondrial potential and swelling assays were performed on rat liver mitochondria (RLM). Mitochondrial membrane potential was measured with the fluorescent probe Safranine O at 580 nm/520 nm upon energization with mitochondrial respiratory chain complex I and II-dependent substrates (glutamate/malate and succinate). Calcium-induced swelling of mitochondria as an index of the MPT was determined. The maximum rate of swelling (V_{\max}) is the quantitative parameter characteristic of this process. Therefore, compounds that effectively decrease V_{\max} are potential inhibitors of the MPT and would be expected to possess neuro(cyto)protective properties.

We have shown that only conjugates **11a–c** with a ditriazole-containing spacer cause some increase of depolarization of RLM with time and slightly potentiate calcium-induced mitochondrial swelling. All other studied bis- γ -carboline do not influence the mitochondrial potential. Moreover, they effectively inhibited in a concentration-dependent manner the calcium-induced mitochondrial swelling of RLM characterizing the process of the MPT (Table 4). Compounds **4b**, **4e**, **8** are the most active as inhibitors of MPT.

It should be noted that the mechanism of antioxidant activity of bis- γ -carboline may be associated not only with radical scavenging but also with inhibition of the MPT and the associated decrease in the production of free radicals. This mechanism of antioxidant activity is characteristic for Dimebon, which does not inhibit Fe^{2+} - and $t\text{BHP}$ -induced LP (Table 3), but it can weakly ($\text{IC}_{50} > 60 \mu\text{M}$) inhibit the spontaneous LP in rat

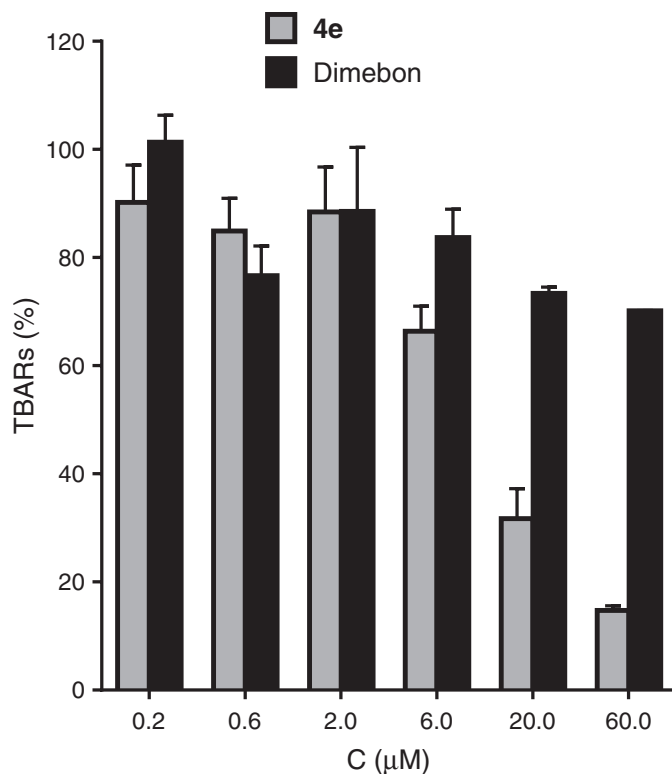


Fig. 4: Influence of compound **4e** on spontaneous lipid peroxidation in rat brain homogenate.

brain homogenate (Fig. 4). For one of the leaders among MPT inhibitory compounds (**4e**), an effective suppression of spontaneous LP in rat brain homogenates with $IC_{50}=10.5\pm 1.3\ \mu\text{M}$ was shown (Fig. 4).

Effect of bis- γ -carbolines on calcium retention capacity of brain mitochondria

Ca^{2+} dysregulation is one of the main features of AD-related cellular pathology. Moreover, it seems obvious that Ca^{2+} retention in mitochondria could play a neuroprotective role by removing excess calcium from the cytoplasm. Therefore, agents that increase mitochondrial calcium retention capacity and, accordingly, increase the threshold of MPT-inducing concentrations of calcium, could improve to some extent the viability of neurons as well as the neuronal activity.

Therefore, we investigated the influence of the leaders in the MPT inhibition test γ -carboline conjugates **4e** and **8**, on calcium retention capacity (CRC) of brain mitochondria (Fig. 5). The experiments were

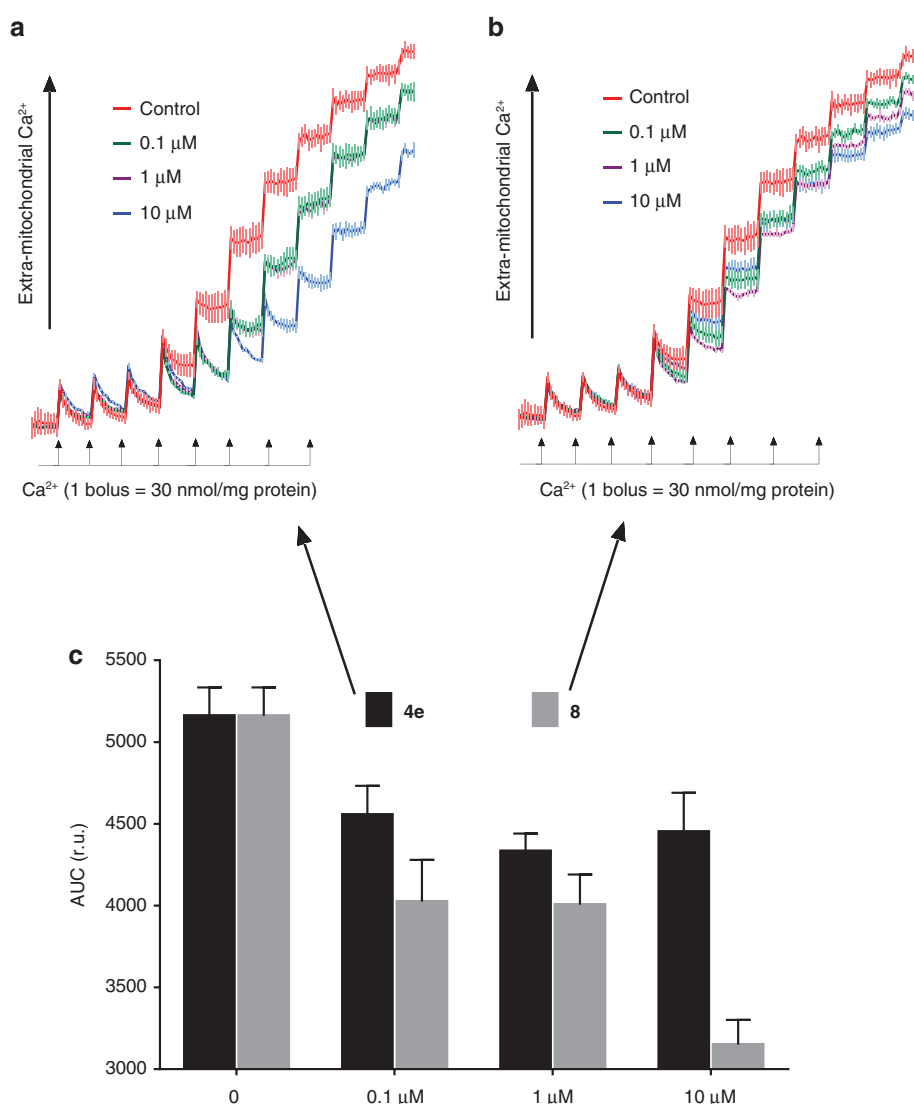


Fig. 5: Influence of compounds **4e** (a) and **8** (b) on calcium retention capacity of mouse brain mitochondria: a and b – kinetics of CaGreen5N fluorescence during the bolus additions of CaCl_2 . c – Area Under the Curve of CaGreen5N fluorescence as an indicator of mitochondrial calcium release, which is inversely proportional to the calcium retention capacity of mitochondria.

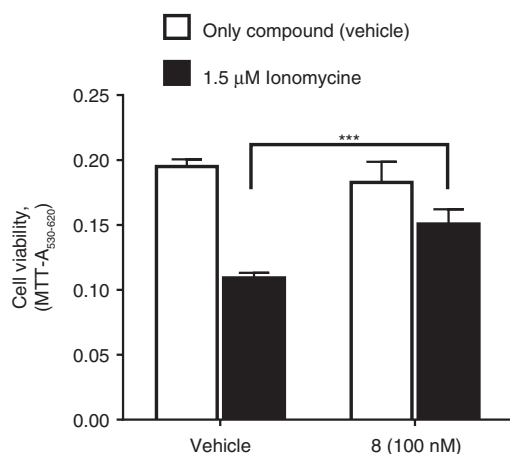


Fig. 6: Effect of compound **8** on cell viability of cerebellar granule neuron in calcium overload cellular model of neurodegeneration. *** $p < 0.0001$, 2-way ANOVA with multiple comparisons.

performed in “bolus” mode [27] with a cell (and mitochondria)-impermeant visible light-excitable Ca^{2+} indicator, Calcium Green-5N.

The increase of probe fluorescence depicted in Fig. 5a, b reflects an increase of extra-mitochondrial calcium and is connected with calcium “bolus” additions, then with decreased uptake of calcium and finally with calcium release from mitochondria due to induction of the MPT. The value of the area under the fluorescence curve (Fig. 5c) can be used as a relative measure characterizing the CRC and inversely proportional to it. One can see from Fig. 5 that compounds **4e** and **8** did not inhibit the initial calcium uptake by brain mitochondria (Fig. 5a, b) and that on the whole, they increased the CRC (Fig. 5a–c).

These results allowed us to assume the neuroprotective potential of conjugates with antioxidant and MPT-inhibition activity. The verification of this assumption was performed with an ionomycin-induced calcium overload model of neuronal death using primary cultures of cerebellar granule cells as described earlier [71]. It was shown (Fig. 6) that compound **8** at 100 nM significantly protected cerebellar granule cells from death in this model of neurodegeneration.

Predicted ADMET and physicochemical profiles of bis- γ -carboline

The results of the computational estimation of a number of ADMET properties for the bis- γ -carboline are shown in Table 5. As can be seen, all the compounds had high predicted values for intestinal absorption,

Table 5: Predicted ADMET and physicochemical profiles of bis- γ -carboline.

Compound	LogBB	HIA, %	hERG, pK_i	hERG, pIC_{50}	LogPow	pS	QED
4a	0.87	80	5.07	5.99	5.16	4.99	0.43
4b	1.28	100	4.90	5.86	5.47	5.37	0.36
4c	0.93	80	5.77	6.49	5.75	5.74	0.32
4d	1.24	100	4.92	5.83	6.01	6.08	0.28
4e	0.32	100	5.60	6.43	5.96	6.22	0.29
8	0.63	85	4.38	5.17	3.97	4.16	0.35
11a	0.10	77	n/p	4.85	3.31	3.67	0.28
11b	0.23	77	n/p	5.00	3.88	4.43	0.21
11c	0.35	77	n/p	4.97	4.49	5.01	0.17
Dimebon	0.76	100	4.76	5.39	4.38	3.96	0.73

LogBB, Blood-brain barrier permeability; HIA, human intestinal absorption [%]; hERG pK_i , hERG potassium channel affinity [$-\log(M)$]; hERG pIC_{50} , hERG potassium channel inhibitory activity [$-\log(M)$]; LogPow, octanol-water partition coefficient; pS, aqueous solubility [$-\log(M)$]; QED, quantitative estimate of drug-likeness; n/p, no prediction.

enabling their oral administration. The conjugates with alkylene linker (**4a–d**) were predicted to have very good blood-brain barrier permeability (brain concentration is about 7–19 times higher than the plasma concentration), ensuring very efficient action on the CNS, although the permeability of other compounds may be more moderate (brain concentration about 1.3–4.3 times higher than the plasma concentration). Both parameters of the cardiac toxicity risk (pK_i and pIC_{50}) for all analyzed compounds (4.38–6.49 log units) are in the lower or medium part of their possible range (3–9 log units). The predicted lipophilicities and aqueous solubilities of the compounds are also good, although some improvement is desirable for a few compounds. Finally, the integral quantitative estimates of drug-likeness (QED) values for most of the compounds were close to 0.3. Thus, the predicted ADMET properties of the studied bis- γ -carbolines are quite acceptable for potential lead compounds at the early drug development stages.

Conclusions

The obtained results show that the synthesized homobivalent Dimebon analogs – bis- γ -carbolines with alkylene, phenylenedialkylene, and triazole-containing spacers exhibit an expanded spectrum of biological activity and improved pharmacological properties compared to their original prototype – Dimebon. Moreover, the compounds with various spacers demonstrate different pharmacological profiles.

Most bis- γ -carbolines, with the exception of compound **11a**, inhibited AChE more efficiently than Dimebon; i.e. the duplication of the γ -carboline molecule increased the inhibitory potency against AChE.

As for the inhibition of BChE, doubling of the γ -carboline pharmacophore in general maintains the rather favorable micromolar anti-BChE activity of Dimebon, with maximum submicromolar activity of **4e**, which has a phenylenedialkylene spacer. Conjugates with long spacers are more active inhibitors of AChE than BChE and demonstrate inversion of selectivity compared with Dimebon.

In contrast to Dimebon, all conjugates displace propidium from the PAS of AChE with maximum activity for **11c**, which has a long ditriazole spacer.

The results of molecular docking reveal the reasons for the increased anti-AChE activity and ability to block AChE-induced aggregation of β -amyloid for the homodimers of γ -carboline, which became double-site inhibitors of AChE, and explain the observed structure-activity relationships for AChE and BChE inhibition.

In contrast to the parent compound Dimebon, all studied bis- γ -carbolines reveal antioxidant activity: they scavenge free radicals in the ABTS test and effectively suppress Fe^{2+} -induced lipid peroxidation. Moreover, conjugates **11a–c** with ditriazole-containing spacers, were the most active antioxidants, both in the ABTS test and in prevention of LP in brain homogenates. In addition, these conjugates had no deleterious effect on the mitochondrial functions that were assessed. The excellent antioxidant, anti-amyloid, and cholinergic potential of these compounds suggest a favorable prospect for the future development of these compounds as medicines for AD treatment.

Whereas conjugates with alkylene (**4a–d**), phenylenedialkylene (**4e**) and monotriazole (**8**) spacers are less active as antioxidants, they effectively prevent the induction of the MPT, increase the calcium retention capacity of mitochondria, and do not influence calcium uptake. MPT inhibition along with antioxidant properties suggest that compounds **4a–e** and **8** could have neuroprotective potential, which was confirmed for **4e** in a cellular calcium overload model of neurodegeneration using cerebellar granule neuron cultures.

The results demonstrate an important role of the spacer that can not only modulate the efficiency of interaction of homobivalent ligands with targets but can also change and determine their pharmacological profile.

The predicted ADMET properties of the studied bis- γ -carbolines showed high values for intestinal absorption and very good blood-brain barrier permeability along with other favorable pharmacokinetic and physico-chemical parameters. This suggests that these new homobivalent Dimebon analogs are quite acceptable as potential lead compounds at the early drug development stages.

Overall, the results showed that new homobivalent Dimebon analogs exhibit an expanded spectrum of biological activity and improved pharmacological properties compared to their prototype. This makes them promising candidates for further research and optimization as multitarget agents for AD treatment.

Methods

General

All chemicals were purchased from Sigma-Aldrich and used without further purification, except as otherwise stated. Solutions were prepared using deionized water (18.2 M Ω cm at 25 °C).

The ^1H NMR spectra were recorded on a Bruker DXP instrument at 200 or 50 MHz, respectively, in CDCl_3 (compounds **3**, **7**, and **10**) and DMSO- d_6 (compounds **4**, **8**, and **11**) using tetramethylsilane as an internal standard. Chemical shifts are reported in ppm units using δ scale. Coupling constants are reported in Hertz (Hz). Melting points were measured in open capillary tubes with a SMP10 melting point apparatus and are uncorrected. The elemental analysis was carried out on an Elementar vario MICRO cube CHN analyzer. Chromatography was carried out on Alfa Aesar Silicagel 60 (0.040–0.063 mm). γ -Carboline **1** was prepared as described in [72]. Dimethanesulfonates **2a–d** were obtained by the procedure reported in [73]. Bismesylate **2e** was purchased from Chemieliva Pharmaceutical Co., Ltd. and used without preliminary purification. The synthesis of compounds **10a–c** was described in [58].

General procedure for the synthesis of bis- γ -carbolines **3a–e**

To a solution of 2 mmol of tetrahydro- γ -carboline **1** in 20 mL of THF, 1.1 mmol of NaH was added. The reaction mixture was stirred for 2 h, and then 1 mmol of methanesulfonate **2** was added. The resulting mixture was stirred at 20 °C for 6 h, then poured into 100 mL of water and extracted with methylene chloride. The solvent was evaporated, and the residue was chromatographed on silica gel (230–400 mesh, eluent hexane–chloroform, 1:4).

1,3-Bis(2,8-dimethyl-3,4-dihydro-1H-pyrido[4,3-b]indol-5(2H)-yl)propane (**3a**)

Isolated yield: 72 %; physical appearance: light brown solid, mp 133–135 °C. ^1H NMR (200 MHz, CDCl_3): δ = 2.13 (quintet, 2H, J = 7.3 Hz, CH_2), 2.43 (s, 6H, MeC), 2.53 (s, 6H, MeN), 2.60–2.84 (m, 8H, CH_2), 3.64 (s, 4H, CH_2), 3.97 (t, 4H, J = 7.3 Hz, CH_2), 6.93 (d, 2H, J = 8.0 Hz, CH_{Ar}), 7.00 (d, 2H, J = 8.0 Hz, CH_{Ar}), 7.20 (s, 2H, CH_{Ar}). Found, %: C, 78.95; H, 8.43; N, 12.87. $\text{C}_{29}\text{H}_{36}\text{N}_4$. Calculated, %: C, 79.05; H, 8.24; N, 12.72.

1,3-Bis(2,8-dimethyl-3,4-dihydro-1H-pyrido[4,3-b]indol-5(2H)-yl)butane (**3b**)

Isolated yield: 67 %; physical appearance: light brown solid, mp 181–183 °C. ^1H NMR (200 MHz, CDCl_3): δ = 1.60–1.80 (m, 4H, CH_2), 2.46 (s, 6H, MeC), 2.57 (s, 6H, MeN), 2.70–2.91 (m, 8H, CH_2), 3.66 (s, 4H, CH_2), 3.84–4.00 (m, 4H, CH_2), 6.97 (d, 2H, J = 8.3 Hz, CH_{Ar}), 7.11 (d, 2H, J = 8.3 Hz, CH_{Ar}), 7.21 (s, 2H, CH_{Ar}). Found, %: C, 79.36; H, 8.57; N, 12.21. $\text{C}_{30}\text{H}_{38}\text{N}_4$. Calculated, %: C, 79.25; H, 8.42; N, 12.32.

1,3-Bis(2,8-dimethyl-3,4-dihydro-1H-pyrido[4,3-b]indol-5(2H)-yl)pentane (**3c**)

Isolated yield: 66 %; physical appearance: light brown solid, mp 120–122 °C. ^1H NMR (200 MHz, CDCl_3): δ = 1.20–1.40 (m, 2H, CH_2), 1.56–1.80 (m, 4H, CH_2), 2.44 (s, 6H, MeC), 2.55 (s, 6H, MeN), 2.79 (s, 8H, CH_2), 3.64

(s, 4H, CH₂), 3.91 (t, 4H, $J=7.1$ Hz, CH₂), 6.94 (d, 2H, $J=8.3$ Hz, CH_{Ar}), 7.11 (d, 2H, $J=8.3$ Hz, CH_{Ar}), 7.19 (s, 2H, CH_{Ar}). Found, %: C, 79.33; H, 8.43; N, 11.78. C₃₁H₄₀N₄. Calculated, %: C, 79.44; H, 8.60; N, 11.95.

1,3-Bis(2,8-dimethyl-3,4-dihydro-1H-pyrido[4,3-b]indol-5(2H)-yl)hexane (3d)

Isolated yield: 56 %; physical appearance: light brown solid, mp 156–158 °C. ¹H NMR (200 MHz, CDCl₃): δ =1.16–1.38 (m, 4H, CH₂), 1.54–1.78 (m, 4H, CH₂), 2.43 (s, 6H, MeC), 2.54 (s, 6H, MeN), 2.79 (s, 8H, CH₂), 3.64 (s, 4H, CH₂), 3.91 (t, 4H, $J=7.1$ Hz, CH₂), 6.94 (d, 2H, $J=8.3$ Hz, CH_{Ar}), 7.09 (d, 2H, $J=8.3$ Hz, CH_{Ar}), 7.18 (s, 2H, CH_{Ar}). Found, %: C, 79.42; H, 8.97; N, 11.73. C₃₂H₄₂N₄. Calculated, %: C, 79.62; H, 8.77; N, 11.61.

1,4-Bis((2,8-dimethyl-3,4-dihydro-1H-pyrido[4,3-b]indol-5(2H)-yl)methyl)benzene (3e)

Isolated yield: 86 %; physical appearance: light brown solid, mp 223–225 °C. ¹H NMR (200 MHz, CDCl₃): δ =2.45 (s, 6H, MeC), 2.57 (s, 6H, MeN), 2.65–2.98 (m, 8H, CH₂), 3.69 (s, 4H, CH₂), 5.15 (s, 4H, PhCH₂), 6.85 (s, 4H, CH_{Ar}), 6.92 (d, 2H, $J=8.2$ Hz, CH_{Ar}), 7.06 (d, 2H, $J=8.2$ Hz, CH_{Ar}), 7.24 (s, 2H, CH_{Ar}). Found, %: C, 81.29; H, 7.51; N, 11.26. C₃₄H₃₈N₄. Calculated, %: C, 81.24; H, 7.62; N, 11.15.

5-((1-(2-(2,8-Dimethyl-3,4-dihydro-1H-pyrido[4,3-b]indol-5(2H)-yl)ethyl)-1H-1,2,3-triazol-4-yl)methyl)-2,8-dimethyl-2,3,4,5-tetrahydro-1H-pyrido[4,3-b]indole (7)

To a solution of 1 mmol of azide **6** in 20 mL of dichloromethane, 1 mmol of *N*-propargylcarboline **5**, 0.1 mmol of CuSO₄ in 1 mL of water, and 0.1 mmol of sodium ascorbate in 1 mL of water were added. The reaction mixture was stirred for 6 h at 40 °C and then washed with 10 mL of a 1 % (v/v) aqueous ammonia solution. The organic layer was separated, dichloromethane was distilled off, and the residue was chromatographed on silica gel (230–400 mesh, methanol–chloroform, 1:10). Isolated yield: 45 %; physical appearance: light brown solid, mp 225–227 °C. ¹H NMR (200 MHz, CDCl₃): δ =2.38 (s, 3H, MeC), 2.42 (s, 3H, MeC), 2.45 (s, 3H, MeN), 2.52 (s, 3H, MeN), 2.22–2.60 (m, 4H, CH₂), 2.77–2.96 (m, 4H, CH₂), 3.47 (s, 2H, CH₂), 3.97 (s, 2H, CH₂), 4.32–4.55 (m, 4H, NCH₂CH₂N), 4.63 (s, 2H, CH₂), 6.37 (s, 1H, NCH=), 6.93 (s, 2H, CH_{Ar}), 6.94 (d, 1H, $J=8.2$ Hz, CH_{Ar}), 7.06 (d, 1H, $J=8.2$ Hz, CH_{Ar}), 7.12 (d, 2H, $J=8.2$ Hz, CH_{Ar}). Found, %: C, 73.47; H, 7.14; N, 19.18. C₃₄H₃₇N₇. Calculated, %: C, 73.34; H, 7.35; N, 19.31.

General procedure for the synthesis of dihydrochlorides of bis- γ -carbolines **4a–e**, **8** and **11a–c**

A 37 % aqueous HCl (0.1 mL) was added to a solution of bis- γ -carboline **3**, **7** or **10** (0.5 mmol) in acetone (2 mL), a precipitate formed was filtered off and recrystallized from 50 % (v/v) aqueous ethanol.

1,3-Bis(2,8-dimethyl-3,4-dihydro-1H-pyrido[4,3-b]indol-5(2H)-yl)propane dihydrochloride (4a)

Isolated yield: 83 %; physical appearance: light brown solid, mp 211–213 °C. ¹H NMR (200 MHz, DMSO-d₆): δ =2.06 (br.s, 2H, CH₂), 2.46 (s, 6H, MeC), 3.03 (s, 6H, MeN), 3.16 (br.s, 4H, CH₂), 3.40–3.66 (m, 2H, CH₂), 3.68–3.90 (m, 2H, CH₂), 4.14–4.48 (m, 6H, CH₂), 4.69 (d, 2H, $J=13.7$ Hz, CH₂), 7.22 (d, 2H, $J=8.5$ Hz, CH_{Ar}), 7.49 (s, 2H, CH_{Ar}), 7.60 (d, 2H, $J=8.5$ Hz, CH_{Ar}), 11.73 (br.s, 2H, NH⁺). Found, %: C, 67.98; H, 7.41; N, 10.82. C₂₉H₃₈Cl₂N₄. Calculated, %: C, 67.82; H, 7.46; N, 10.91.

1,3-Bis(2,8-dimethyl-3,4-dihydro-1H-pyrido[4,3-b]indol-5(2H)-yl)butane dihydrochloride (4b)

Isolated yield: 77 %; physical appearance: light brown solid, mp 292–294 °C. ¹H NMR (200 MHz, DMSO-d₆): δ =1.50–1.87 (m, 4H, CH₂), 2.39 (s, 6H, MeC), 2.91 (s, 6H, MeN), 3.06 (br.s, 4H, CH₂), 3.40–3.66 (m, 2H, CH₂), 3.68–3.90 (m, 2H, CH₂), 4.06–4.48 (m, 6H, CH₂), 4.64 (d, 2H, $J=13.7$ Hz, CH₂), 6.97 (d, 2H, $J=7.8$ Hz, CH_{Ar}),

7.21 (s, 2H, CH_{Ar}), 7.33 (d, 2H, $J=7.8$ Hz, CH_{Ar}), 11.30 (br.s, 2H, NH⁺). Found, %: C, 68.53; H, 7.47; N, 10.44. C₃₀H₄₀Cl₂N₄. Calculated, %: C, 68.30; H, 7.64; N, 10.62.

1,3-Bis(2,8-dimethyl-3,4-dihydro-1H-pyrido[4,3-b]indol-5(2H)-yl)pentane dihydrochloride (4c)

Isolated yield: 76 %; physical appearance: light brown solid, mp 144–146 °C. ¹H NMR (200 MHz, DMSO-d₆): δ =1.18–1.44 (m, 2H, CH₂), 1.56–1.86 (m, 4H, CH₂), 2.47 (s, 6H, MeC), 3.04 (s, 6H, MeN), 3.42–3.66 (m, 4H, CH₂), 3.64–3.94 (m, 4H, CH₂), 4.08–4.48 (m, 6H, CH₂), 4.69 (d, 2H, $J=14.0$ Hz, CH₂), 7.24 (d, 2H, $J=7.8$ Hz, CH_{Ar}), 7.48 (s, 2H, CH_{Ar}), 7.60 (d, 2H, $J=7.8$ Hz, CH_{Ar}), 11.65 (br.s, 2H, NH⁺). Found, %: C, 68.87; H, 7.96; N, 10.52. C₃₁H₄₂Cl₂N₄. Calculated, %: C, 68.75; H, 7.82; N, 10.34.

1,3-Bis(2,8-dimethyl-3,4-dihydro-1H-pyrido[4,3-b]indol-5(2H)-yl)hexane dihydrochloride (4d)

Isolated yield: 71 %; physical appearance: light brown solid, mp 176–178 °C. ¹H NMR (200 MHz, DMSO-d₆): δ =1.16–1.40 (m, 4H, CH₂), 1.52–1.80 (m, 4H, CH₂), 2.46 (s, 6H, MeC), 3.02 (s, 6H, MeN), 3.40–3.65 (m, 4H, CH₂), 3.64–3.94 (m, 4H, CH₂), 4.04–4.27 (m, 4H, CH₂), 4.28–4.46 (m, 2H, CH₂), 4.67 (d, 2H, $J=13.0$ Hz, CH₂), 7.20 (d, 2H, $J=7.8$ Hz, CH_{Ar}), 7.47 (s, 2H, CH_{Ar}), 7.58 (d, 2H, $J=7.8$ Hz, CH_{Ar}), 11.77 (br.s, 2H, NH⁺). Found, %: C, 69.31; H, 8.08; N, 10.17. C₃₂H₄₄Cl₂N₄. Calculated, %: C, 69.17; H, 7.98; N, 10.08.

1,4-Bis((2,8-dimethyl-3,4-dihydro-1H-pyrido[4,3-b]indol-5(2H)-yl)methyl)benzene dihydrochloride (4e)

Isolated yield: 81 %; physical appearance: light brown solid, mp 294–255 °C. ¹H NMR (200 MHz, DMSO-d₆): δ =2.34 (s, 6H, MeC), 2.91 (s, 6H, MeN), 3.05 (br.s, 4H, CH₂), 3.58–3.77 (m, 4H, CH₂), 4.12–4.30 (m, 2H, CH₂), 4.53 (d, 2H, $J=13.6$ Hz, CH₂), 5.22, 5.35 (AB system, 4H, $J_{AB}=16.9$ Hz, PhCH₂), 6.90 (d, 2H, $J=8.3$ Hz, CH_{Ar}), 6.95 (s, 4H, CH_{Ar}), 7.20 (s, 2H, CH_{Ar}), 7.27 (d, 2H, $J=8.3$ Hz, CH_{Ar}), 10.95 (br.s, 2H, NH⁺). Found, %: C, 71.03; H, 7.09; N, 9.64. C₃₄H₄₀Cl₂N₄. Calculated, %: C, 70.94; H, 7.00; N, 9.73.

5-((1-(2-(2,8-Dimethyl-3,4-dihydro-1H-pyrido[4,3-b]indol-5(2H)-yl)ethyl)-1H-1,2,3-triazol-4-yl)methyl)-2,8-dimethyl-2,3,4,5-tetrahydro-1H-pyrido[4,3-b]indole dihydrochloride (8)

Isolated yield: 63 %; physical appearance: brown solid, mp 294–296. ¹H NMR (200 MHz, DMSO-d₆): δ =2.37 (s, 6H, MeC), 2.67–2.88 (s + m, 5H, MeN + CH₂), 3.02 (s, 3H, MeN), 3.14–3.43 (m, 6H, CH₂), 3.54–3.82 (m, 4H, CH₂), 3.93 (s, 2H, CH₂), 4.29–4.75 (m, 4H, CH₂), 6.91 (d, 1H, $J=8.6$ Hz, CH_{Ar}), 7.00 (d, 1H, $J=8.6$ Hz, CH_{Ar}), 7.19 (s, 1H, CH_{Ar}), 7.20 (d, 1H, $J=8.5$ Hz, CH_{Ar}), 7.31 (s, 1H, CH_{Ar}), 7.32 (d, 1H, $J=8.5$ Hz, CH_{Ar}), 7.57 (s, 1H, NCH=), 11.20 (br.s, 2H, NH⁺). Found, %: C, 64.23; H, 6.86; Cl, 12.42; N, 16.89. C₃₁H₃₉Cl₂N₇. Calculated, %: C, 64.13; H, 6.77; Cl, 12.21; N, 16.89.

1,2-Bis(4-((2,8-dimethyl-3,4-dihydro-1H-pyrido[4,3-b]indol-5(2H)-yl)methyl)-1H-1,2,3-triazol-1-yl)ethane dihydrochloride (11a)

Isolated yield: 62 %; physical appearance: brown solid, mp 227–228. ¹H NMR (200 MHz, DMSO-d₆): δ =2.46 (s, 6H, MeC), 3.07 (s, 6H, MeN), 3.16–3.40 (m, 8H, CH₂), 3.56–3.98 (m, 4H, CH₂), 4.07 (s, 4H, CH₂), 4.93 (s, 4H, CH₂), 7.23 (d, 2H, $J=8.5$ Hz, CH_{Ar}), 7.56 (s, 2H, CH_{Ar}), 7.57 (d, 2H, $J=8.5$ Hz, CH_{Ar}), 8.00 (s, 2H, NCH=), 12.77 (br.s, 2H, NH⁺). Found, %: C, 61.89; H, 6.57; N, 21.01. C₃₄H₄₂Cl₂N₁₀. Calculated, %: C, 61.72; H, 6.40; N, 21.17.

1,2-Bis(4-((2,8-dimethyl-3,4-dihydro-1H-pyrido[4,3-b]indol-5(2H)-yl)methyl)-1H-1,2,3-triazol-1-yl)butane dihydrochloride (11b)

Isolated yield: 73 %; physical appearance: brown solid, mp 210–211. ¹H NMR (200 MHz, DMSO-d₆): δ =1.54–1.92 (m, 4H, CH₂), 2.43 (s, 6H, MeC), 3.07 (s, 6H, MeN), 3.32–3.54 (m, 8H, CH₂), 3.56–3.94 (m, 4H, CH₂), 4.08–4.48

(m, 6H, CH₂), 4.69 (d, 2H, J =14.0 Hz, CH₂), 7.22 (d, 2H, J =7.8 Hz, CH_{Ar}), 7.57 (s, 2H, CH_{Ar}), 7.58 (d, 2H, J =7.8 Hz, CH_{Ar}), 8.11 (s, 2H, NCH=), 11.62 (br.s, 2H, NH⁺). Found, %: C, 62.48; H, 6.67; N, 20.42. C₃₆H₄₆Cl₂N₁₀. Calculated, %: C, 62.69; H, 6.72; N, 20.31.

1,2-Bis(4-((2,8-dimethyl-3,4-dihydro-1H-pyrido[4,3-b]indol-5(2H)-yl)methyl)-1H-1,2,3-triazol-1-yl)hexane dihydrochloride (11c)

Isolated yield: 56 %; physical appearance: brown solid, mp 194–196. ¹H NMR (200 MHz, DMSO-d₆): δ =1.06–1.33 (m, 4H, CH₂), 1.58–1.88 (m, 4H, CH₂), 2.43 (s, 6H, MeC), 3.05 (s, 6H, MeN), 3.40–3.65 (m, 8H, CH₂), 3.64–3.94 (m, 6H, CH₂), 4.23–4.51 (m, 4H, CH₂), 4.70 (d, 2H, J =13.0 Hz, CH₂), 5.56 (s, 2H, CH₂), 7.22 (d, 2H, J =8.5 Hz, CH_{Ar}), 7.46 (s, 2H, CH_{Ar}), 7.76 (d, 2H, J =8.5 Hz, CH_{Ar}), 8.36 (s, 2H, NCH=), 11.52 (br.s, 2H, NH⁺). Found, %: C, 63.72; H, 6.92; N, 19.26. C₃₈H₅₀Cl₂N₁₀. Calculated, %: C, 63.59; H, 7.02; N, 19.51.

Biological assay

Enzymatic assays

In vitro AChE, BChE and CES inhibition

All experiments were carried out in accordance with the standard protocols approved by IPAC RAS.

Human erythrocyte acetylcholinesterase (AChE), equine serum butyrylcholinesterase (BChE), porcine liver carboxylesterase (CES), acetylthiocholine iodide (ATCh), butyrylthiocholine iodide (BTCh), 5,5'-dithio-bis-(2-nitrobenzoic acid) (DTNB), and 4-nitrophenol acetate (4-NPA) were purchased from Sigma-Aldrich. AChE and BChE activities were measured by the colorimetric method of Ellman *et al.* [74] with some minor modifications as described in detail in [65]. The assay solution consisted of 0.1 M K/Na phosphate buffer pH 7.5, 25 °C, 0.33 mM DTNB, 0.02 unit/mL AChE or BChE, and 1 mM substrate (ATCh or BTCh, respectively). Reagent blanks consisted of reaction mixtures without substrates. The activity of CES was determined spectrophotometrically by the release of 4-nitrophenol at 405 nm [75] in 0.1 M K/Na phosphate buffer pH 8.0, 25 °C as described in detail in [65]. Final enzyme and substrate (4-nitrophenyl acetate) concentrations were 0.02 unit/mL and 1 mM, respectively. Assays were carried out with a blank containing all constituents except porcine CES to assess non-enzymatic hydrolysis.

Test compounds were dissolved in DMSO; reaction mixtures contained 2 % (v/v) of the solvent, a concentration shown not to affect the activity of the enzymes on its own (data not shown). An initial evaluation of inhibitory activity of compounds was carried out by determination of the AChE, BChE, and CES inhibition at a compound concentration of 20 μ M. For this, a sample of the corresponding enzyme was incubated with the test compound for 5 min; then the enzyme residual activity was determined. Each experiment was performed in triplicate.

The most active compounds were then selected for determination of IC₅₀ (inhibitor concentration resulting in 50 % inhibition of control enzyme activity). Compounds (eight concentrations ranging between 10⁻¹² and 10⁻⁴ M were selected to achieve 20 to 80 % inhibition) were incubated with each enzyme for 5 min at 25 °C. Substrate was then added and residual enzyme activity relative to an inhibitor-free control was measured using a FLUOStar OPTIMA (BMG Labtech, Germany) microplate reader. Origin 6.1 for Windows was used to determine IC₅₀ values from plots of log (inhibitor concentration) vs. % (residual activity). Results were expressed as mean \pm SEM (n = 3 experiments).

Kinetic analysis of AChE and BChE inhibition. Determination of steady-state inhibition constants

To elucidate mechanism of AChE and BChE inhibition by bis- γ -carbolines, the enzymes' residual activity was measured in the presence of three increasing concentrations of the test compounds and six decreasing

concentrations of the substrates. The test compounds were preincubated with the enzymes at 25 °C for 5 min, followed by the addition of the substrates. Parallel controls were made for an assay of the rate of hydrolysis of the same concentrations of substrates in the solutions with no inhibitor. Measurements were performed using a FLUOStar OPTIMA (BMG Labtech Germany) microplate reader. Inhibition constants K_i (competitive component) and αK_i (noncompetitive component) were determined by linear regression of $1/V$ vs. $1/[S]$ double-reciprocal (Lineweaver-Burk) plots using Origin 6.1 software. Data were expressed as mean \pm SEM ($n=3$ experiments).

Propidium displacement studies

The ability of the test compounds to competitively displace propidium, a selective ligand of the PAS of AChE, was evaluated by a fluorescence method [67, 76] with some minor modifications as described in detail in [35]. *EeAChE* was used owing to its high degree of purification, high activity, and lower cost than human AChE (hAChE). In addition, we performed a 3D alignment of the crystal structures of *EeAChE* (PDB 1C2O) and hAChE (PDB 4EY7) using YASARA-Structure 18.4.24 for Windows, which showed that the two structures were essentially congruent with an RMSD of 0.623 Å over 527 aligned residues and 88.6 % sequence identity. The fluorescence intensity of propidium iodide bound with AChE increases several times. A decrease in propidium fluorescence in the presence of test compounds suggests that they are able to displace propidium and can bind to the PAS of AChE [15]. To determine the degree of displacement (% displacement) of propidium from the PAS of AChE, *EeAChE* (final concentration, 7 μ M) was incubated with the test compound at a concentration of 20 μ M in 1 mM Tris-HCl buffer pH 8.0, 25 °C, for 15 min. Then, propidium iodide solution (final concentration, 8 μ M) was added, the samples were incubated for 15 min and the fluorescence spectrum (530 nm (excitation) and 600 nm (emission)) was taken. Donepezil was used as a reference compound. The blank contained propidium iodide of the same concentration in 1 mM Tris-HCl buffer pH 8.0. The measurements were carried out in triplicate on a microplate reader FLUOStar Optima (BMG Labtech, Germany), and the results calculated by the following formula:

$$\% \text{ Displacement} = 100 - \left(\text{IF}_{\text{AChE} + \text{Propidium} + \text{inhibitor}} / \text{IF}_{\text{AChE} + \text{Propidium}} \right) \times 100,$$

where $\text{IF}_{\text{AChE} + \text{Propidium}}$ is the fluorescence intensity of the propidium associated with AChE in the absence of the test compound (taken as 100 %), and $\text{IF}_{\text{AChE} + \text{Propidium} + \text{inhibitor}}$ is the fluorescence intensity of the propidium associated with AChE in the presence of the test compound.

ABTS radical cation scavenging activity assay

Radical scavenging activity of the compounds was assessed using an ABTS radical decolorization assay [69] with some minor modifications as described in detail in [35]. ABTS (2,2'-azino-bis-(3-ethylbenzothiazoline-6-sulfonic acid) diammonium salt) was purchased from TCI (Tokyo, Japan); potassium persulfate (di-potassium peroxodisulfate) and Trolox (6-hydroxy-2,5,7,8-tetramethylchroman-2-carboxylic acid) were obtained from Sigma-Aldrich Chemical Co. (St. Louis, MO, USA). Ethanol was HPLC grade. Aqueous solutions were prepared using deionized water. Trolox was used as the antioxidant standard.

Radical scavenging activity of compounds was determined by measuring the decrease in absorbance at 734 nm 1 h after mixing 10 μ L of test compound solution with 240 μ L of ABTS $^{+}$ working solution in ethanol (100 μ M final concentration) using a Bio-Rad xMark microplate UV/VIS spectrophotometer vs. ethanol blanks. Antioxidant activity was expressed as Trolox equivalent antioxidant capacity (TEAC) values (ratios between slopes of linear correlations for concentrations of test compounds and Trolox with absorbance of the ABTS radical). The compounds were tested in the concentration range of 1×10^{-6} – 1×10^{-4} M. IC_{50} values (concentrations required to reduce 50 % of the ABTS radical) were determined for the most active compounds

using Origin 6.1 for Windows (OriginLab, Northampton, MA, USA). Values were obtained from three replicates of each sample and three independent experiments.

Rat liver and brain mitochondria isolation

Rat livers were isolated from adult Wistar strain rats aged 3.5–4 months (250–350 g) fasted overnight. Rats were anesthetized with carbon dioxide and killed by decapitation. The isolation of rat liver mitochondria was carried out by conventional differential centrifugation in an ice-cold isolation buffer (IB), pH 7.6: 75 mM sucrose, 225 mM mannitol, 10 mM K-HEPES with addition of 0.5 mM EGTA, 0.5 mM EDTA and 1 mg/mL BSA. Mouse brain nonsynaptosomal mitochondria were isolated by centrifugation in a Percoll gradient [27]. In brief: mice were euthanized by cervical dislocation and the brains were quickly removed, homogenized in an ice-cold IB pH 7.4 and the homogenate was centrifuged for 11 min at $1500\times g$. The pellet was homogenized in half of the volume of the same buffer and centrifugation was repeated. The combined supernatants were centrifuged at $10,500\times g$ for 11 min. The resulting pellet was resuspended in 12 % (w/v) Percoll, layered onto a Percoll gradient (40 %–23 % w/v) and centrifuged at $30,700\times g$ at 4 °C for 15 min. The mitochondrial layer was collected and washed twice using centrifugation. The final pellet was resuspended in the IB containing 0.02 mM EGTA. The mitochondrial protein concentration was determined using a biuret procedure with BSA as a standard [77].

Lipid peroxidation

The effect of the compounds on lipid peroxidation (LP) was determined using a crude membrane fraction of rat brain homogenate obtained by standard methods in a buffer (0.12 M HEPES, 0.1 M KCl), pH 7.5. The degree of LP was measured using the thiobarbituric reagent and estimated by the level of thiobarbituric acid reactive substances (TBARs) [78]. The incubation medium for the determination of LP contained a suspension of membranes in a buffer at a final concentration of 1–2 mg of protein per mL and various concentrations of the test compounds or a solvent (DMSO) in control samples. Protein concentration in the membrane suspension was determined by the biuret method using BSA as a standard [77]. The lipid peroxidation reaction was initiated by Fe^{2+} ions ($\text{Fe}_2\text{SO}_4 \times 7\text{H}_2\text{O}$ at a final concentration of 0.5 mM) or by *tert*-butylhydroperoxide (1.6 mM, tBHP), followed by incubation at 37 °C for 30 min. To assess spontaneous LP, the homogenate was incubated for 2 h at 37 °C in the presence of compounds or an equal volume of solvent. The LP reaction was stopped by introducing into the incubation medium a reagent containing 250 mM HCl, 15 % (w/v) trichloroacetic acid and 3 mM thiobarbituric acid. The reaction samples were incubated at 90 °C for 60 min. Then the samples were centrifuged for 10 min at $10,000\times g$, the supernatants were transferred to a 96-well plate, and the difference in optical absorbance measured at wavelengths of 530 nm and 620 nm was determined on a Wallac Victor 1420 Multilabel Counter (Perkin Elmer) plate spectrophotometer. The results were expressed as a percentage of the optical absorption of the samples in the presence of the test compounds to the optical absorption of the control samples. The IC_{50} values for antioxidant activities of compounds were calculated using Origin 6.1 for Windows (OriginLab, Northampton, MA, USA) and presented as mean \pm SEM.

Mitochondrial potential and permeability transition

Safranin O (10 μM) was used as a membrane potential probe [79]. Fluorescence intensity at 580 nm (excitation at 520 nm) was measured with Victor3 multi-well fluorescence plate reader (Perkin Elmer, Germany). Mitochondrial protein concentration was 0.2 mg/mL. The medium for measurements contained 75 mM sucrose, 225 mM mannitol, 10 mM K-HEPES (pH 7.4), 0.02 mM EGTA, 1 mM KH_2PO_4 . After a 5-min incubation, substrates of respiratory activity (5 mM glutamate/malate or 5 mM succinate and the inhibitor of complex I, 0.5

μM rotenone) were added to produce the mitochondrial potential. Then the compounds ($30\ \mu\text{M}$) or the same volume of vehicle (DMSO) were injected into the mitochondrial suspension. After 15–20 min, $12.5\ \mu\text{M}$ CaCl_2 was added to each probe to induce the depolarization of mitochondria and $0.5\ \mu\text{M}$ FCCP (carbonyl cyanide *p*-trifluoromethoxyphenyl hydrazone) was finally added to achieve maximum depolarization. Results on mitochondrial membrane potential were presented as the normalized mean \pm SD for mitochondrial potential measurements between the level of potential after addition of the substrate and maximum depolarization after addition of the FCCP.

Ca^{2+} -induced mitochondrial swelling was used to study the mitochondrial permeability transition induction. The mitochondrial swelling was determined by monitoring the absorbance at 620 nm using a Victor3 multi-well fluorescence plate reader (Perkin Elmer, Germany). The rat liver mitochondria ($0.2\ \text{mg/mL}$) were incubated in a buffer containing 75 mM sucrose, 225 mM mannitol, 10 mM K-HEPES (pH 7.4), 0.02 mM EGTA, 1 mM KH_2PO_4 , 5 mM succinate, and $0.5\ \mu\text{M}$ rotenone for energized conditions. The mitochondrial suspensions ($0.2\ \text{mg/mL}$) were infused with the $25\ \mu\text{M}$ CaCl_2 solution. The results were expressed as a percentage of the maximum rate of absorption decline ($\text{dA}_{620}/\text{dt}$, %) in the samples in the presence of the test compounds to the maximum rate of absorption decline ($\text{dA}_{620}/\text{dt}$, 100 %) in the control samples. The IC_{50} values were calculated using Origin 6.1 for Windows (OriginLab, Northampton, MA, USA) and presented as mean \pm SEM. All experiments with mitochondria were repeated in at least five separate preparations.

Evaluation of calcium retention capacity of brain mitochondria

Calcium retention capacity was evaluated in the KCl-based medium supplemented with 100 nM Calcium Green-5N (Molecular Probes) using a EnVision multi-well fluorescence plate reader (Perkin Elmer, Germany) with $\text{ex/em} = 506/535\ \text{nm}$. The brain mitochondria ($0.2\ \text{mg/mL}$) were suspended in the KCl-based medium (120 mM KCl, 20 mM HEPES, 100 mM sucrose, 0.2 mM KH_2PO_4 , 0.45 mM MgCl_2 , pH 7.2), containing 5 mM succinate, $1\ \mu\text{M}$ rotenone, 0.15 mM ADP and $1\ \mu\text{g/mL}$ oligomycin. Experiments were carried out in 96 well plates at $30\ ^\circ\text{C}$. Calcium addition in “bolus mode” was used. All figures with fluorescence kinetic during the calcium additions are representative of at least three separate, independent experiments. Experiments were replicated in at least three separate mitochondria preparations.

Molecular modeling

For molecular modeling, geometries of the structures, with the tertiary amino-groups protonated, were QM-optimized with GAMESS-US [80] software (B3LYP/6-31G*). For molecular docking, the optimized structures of the ligands were used with partial atomic charges derived from QM results according to the Mulliken scheme [81].

X-ray crystal structures of human AChE PDB: 4EY4 (apo-state) and PDB:4EY7 (co-crystallized with Donepezil) [82] were used for molecular docking after removal of waters and other ligands.

Molecular docking with a Lamarckian Genetic Algorithm (LGA) [83] was performed with AutoDock 4.2.6 software [84]. The grid box for docking included the entire active site gorge of AChE ($22.5\text{\AA} \times 22.5\text{\AA} \times 22.5\text{\AA}$ grid box dimensions with grid spacing of 0.375\AA). The main LGA parameters were 256 runs, 25×10^6 evaluations, 27×10^4 generations and a population size of 3000.

Prediction of ADMET and physicochemical profiles

Human intestinal absorption (HIA) [85], blood-brain barrier permeability (LogBB) [86], and hERG-mediated cardiac toxicity risk (channel affinity pK_i and inhibitory activity pIC_{50}) [87] were estimated using

the integrated online service for ADMET properties prediction ADMET Prediction Service [88] (<http://qsar.chem.msu.ru/admet/>). It implements the predictive QSAR models based on accurate and representative training sets, fragmental descriptors, and artificial neural networks. The lipophilicity (LogPow) and aqueous solubility (pS) were estimated by the ALogPS 3.0 neural network model implemented in the OCHEM platform [89]. The quantitative estimate of drug-likeness (QED) values [90] were calculated by the RDKit version 2019.03.4 software [91].

Acknowledgements: This work was supported by the IPAC RAS State Targets Project # 0090-2019-0005. Part of this work connected with synthesis of chemical compounds was supported by grant of Russian Science Foundation #19-13-00378. Computer modeling was carried out using equipment from the shared research facilities of the HPC computing resources at Lomonosov Moscow State University [92]. The equipment of the “Centre for Collective Use of IPAC RAS” was used. Support for RJR’s contributions was provided by an Mcubed grant and other resources of the University of Michigan. The funding sources had no role in the study design; collection, analysis and interpretation of data; writing of the manuscript; or the decision to submit the article for publication.

Conflicts of interest: There are no conflicts to declare.

References

- [1] Alzheimer’s Association. *Alzheimers Dement.* **11**, 332 (2015).
- [2] M. L. Bolognesi, R. Matera, A. Minarini, M. Rosini, C. Melchiorre. *Curr. Opin. Chem. Biol.* **13**, 303 (2009).
- [3] S. O. Bachurin, E. V. Bovina, A. A. Ustyugov. *Med. Res. Rev.* **37**, 1186 (2017).
- [4] J. F. Gonzalez, A. R. Alcantara, A. L. Doadrio, J. M. Sanchez-Montero. *Expert Opin. Drug Discov.* **14**, 879 (2019).
- [5] Y. Furukawa-Hibi, T. Alkam, A. Nitta, A. Matsuyama, H. Mizoguchi, K. Suzuki, S. Moussaoui, Q. S. Yu, N. H. Greig, T. Nagai, K. Yamada. *Behav. Brain. Res.* **225**, 222 (2011).
- [6] A. Nordberg, C. Ballard, R. Bullock, T. Darreh-Shori, M. Somogyi. *Prim. Care Companion CNS Disord.* **15**, PCC.12r01412 (2013).
- [7] R. M. Lane, S. G. Potkin, A. Enz. *Int. J. Neuropsychopharmacol.* **9**, 101 (2006).
- [8] G. V. De Ferrari, M. A. Canales, I. Shin, L. M. Weiner, I. Silman, N. C. Inestrosa. *Biochemistry* **40**, 10447 (2001).
- [9] A. Alvarez, C. Opazo, R. Alarcon, J. Garrido, N. C. Inestrosa. *J. Mol. Biol.* **272**, 348 (1997).
- [10] M. Bartolini, C. Bertucci, V. Cavrini, V. Andrisano. *Biochem. Pharmacol.* **65**, 407 (2003).
- [11] S. V. Lushchekina, E. D. Kots, D. A. Novichkova, K. A. Petrov, P. Masson. *J. Bionanosci.* **7**, 396 (2016).
- [12] N. C. Inestrosa, A. Alvarez, C. A. Pérez, R. D. Moreno, M. Vicente, C. Linker, O. I. Casanueva, C. Soto, J. Garrido. *Neuron* **16**, 881 (1996).
- [13] N. C. Inestrosa, M. C. Dinamarca, A. Alvarez. *FEBS J.* **275**, 625 (2008).
- [14] P. Muñoz-Ruiz, L. Rubio, E. García-Palomero, I. Dorronsoro, M. del Monte-Millán, R. Valenzuela, P. Usán, C. de Austria, M. Bartolini, V. Andrisano, A. Bidon-Chanal, M. Orozco, F. J. Luque, M. Medina, A. Martínez. *J. Med. Chem.* **48**, 7223 (2005).
- [15] M. P. Arce, M. I. Rodríguez-Franco, G. C. Gonzalez-Munoz, C. Perez, B. Lopez, M. Villarroja, M. G. Lopez, A. G. Garcia, S. Conde. *J. Med. Chem.* **52**, 7249 (2009).
- [16] P. Camps, X. Formosa, C. Galdeano, T. Gomez, D. Munoz-Torrero, L. Ramirez, E. Viayna, E. Gomez, N. Isambert, R. Lavilla, A. Badia, M. V. Clos, M. Bartolini, F. Mancini, V. Andrisano, A. Bidon-Chanal, O. Huertas, T. Dafni, F. J. Luque. *Chem. Biol. Interact.* **187**, 411 (2010).
- [17] J. Rouleau, B. I. Iorga, C. Guillou. *Eur. J. Med. Chem.* **46**, 2193 (2011).
- [18] I. Zueva, J. Dias, S. Lushchekina, V. Semenov, M. Mukhamedyarov, T. Pashirova, V. Babaev, F. Nachon, N. Petrova, L. Nurullin, L. Zakharova, V. Ilyin, P. Masson, K. Petrov. *Neuropharmacology* **155**, 131 (2019).
- [19] M. M. Mesulam, C. Geula. *Ann. Neurol.* **36**, 722 (1994).
- [20] V. K. Ramanan, S. L. Risacher, K. Nho, S. Kim, S. Swaminathan, L. Shen, T. M. Foroud, H. Hakonarson, M. J. Huentelman, P. S. Aisen, R. C. Petersen, R. C. Green, C. R. Jack, R. A. Koeppe, W. J. Jagust, M. W. Weiner, A. J. Saykin. *Mol. Psychiatry* **19**, 351 (2014).
- [21] S. Darvesh. *Curr. Alzheimer Res.* **13**, 1 (2016).
- [22] E. Radi, P. Formichi, C. Battisti, A. Federico. *J. Alzheimers. Dis.* **42 Suppl 3**, S125 (2014).
- [23] W. J. Huang, X. Zhang, W. W. Chen. *Biomed. Rep.* **4**, 519 (2016).
- [24] M. G. Savelieff, G. Nam, J. Kang, H. J. Lee, M. Lee, M. H. Lim. *Chem. Rev.* **119**, 1221 (2018).

- [25] M. Pohanka. *Bratisl. Lek. Listy* **119**, 535 (2018).
- [26] G. Ganguly, S. Chakrabarti, U. Chatterjee, L. Saso. *Drug Des. Devel. Ther.* **11**, 797 (2017).
- [27] E. F. Shevtsova, D. V. Vinogradova, E. G. Kireeva, V. P. Reddy, G. Aliev, S. O. Bachurin. *Curr. Alzheimer Res.* **11**, 422 (2014).
- [28] E. F. Shevtsova, D. V. Vinogradova, M. E. Neganova, M. Avila-Rodriguez, G. M. Ashraf, G. E. Barreto, S. O. Bachurin, G. Aliev. *CNS Neurol. Disord. Drug Targets* **16**, 677 (2017).
- [29] A. Cavalli, M. L. Bolognesi, A. Minarini, M. Rosini, V. Tumiatti, M. Recanatini, C. Melchiorre. *J. Med. Chem.* **51**, 347 (2008).
- [30] M. Rosini, E. Simoni, A. Minarini, C. Melchiorre. *Neurochem. Res.* **39**, 1914 (2014).
- [31] A. Agis-Torres, M. Solhuber, M. Fernandez, J. M. Sanchez-Montero. *Curr. Neuropharmacol.* **12**, 2 (2014).
- [32] K. S. Dias, C. Viegas, Jr. *Curr. Neuropharmacol.* **12**, 239 (2014).
- [33] G. F. Makhaeva, S. V. Lushchekina, N. P. Boltneva, V. B. Sokolov, V. V. Grigoriev, O. G. Serebryakova, E. A. Vikhareva, A. Y. Aksinenko, G. E. Barreto, G. Aliev, S. O. Bachurin. *Sci. Rep.* **5**, 13164 (2015).
- [34] S. O. Bachurin, E. F. Shevtsova, G. F. Makhaeva, V. V. Grigoriev, N. P. Boltneva, N. V. Kovaleva, S. V. Lushchekina, P. N. Shevtsov, M. E. Neganova, O. M. Redkozubova, E. V. Bovina, A. V. Gabrelyan, V. P. Fisenko, V. B. Sokolov, A. Y. Aksinenko, V. Echeverria, G. E. Barreto, G. Aliev. *Sci. Rep.* **7**, 45627 (2017).
- [35] S. O. Bachurin, G. F. Makhaeva, E. F. Shevtsova, N. P. Boltneva, N. V. Kovaleva, S. V. Lushchekina, E. V. Rudakova, L. G. Dubova, D. V. Vinogradova, V. B. Sokolov, A. Y. Aksinenko, V. P. Fisenko, R. J. Richardson, G. Aliev. *Sci. Rep.* **9**, 4873 (2019).
- [36] G. F. Makhaeva, E. F. Shevtsova, N. P. Boltneva, S. V. Lushchekina, N. V. Kovaleva, E. V. Rudakova, S. O. Bachurin, R. J. Richardson. *Chem. Biol. Interact.* **308**, 224 (2019).
- [37] M. Benchekroun, S. Maramai. *Future Med. Chem.* **11**, 261 (2019).
- [38] F. Prati, E. Uliassi, M. L. Bolognesi. *MedChemComm* **5**, 853 (2014).
- [39] R. R. Ramsay, M. R. Popovic-Nikolic, K. Nikolic, E. Uliassi, M. L. Bolognesi. *Clin. Transl. Med.* **7**, 3 (2018).
- [40] M. L. Bolognesi. *ACS Med. Chem. Lett.* **10**, 273 (2019).
- [41] M. L. Bolognesi, A. Cavalli. *ChemMedChem* **11**, 1190 (2016).
- [42] M. Decker. *J. Med. Chem.* **49**, 5411 (2006).
- [43] M. Rosini, E. Simoni, M. Bartolini, E. Soriano, J. Marco-Contelles, V. Andrisano, B. Monti, M. Windisch, B. Hutter-Paier, D. W. McClymont, I. R. Mellor, M. L. Bolognesi. *ChemMedChem* **8**, 1276 (2013).
- [44] Y. Zhao, F. Ye, J. Xu, Q. Liao, L. Chen, W. Zhang, H. Sun, W. Liu, F. Feng, W. Qu. *Bioorg. Med. Chem.* **26**, 3812 (2018).
- [45] R. Leon, A. G. Garcia, J. Marco-Contelles. *Med. Res. Rev.* **33**, 139 (2013).
- [46] Y.-P. Pang, P. Quiram, T. Jelacic, F. Hong, S. Brimijoin. *J. Biol. Chem.* **271**, 23646 (1996).
- [47] C. Guillou, A. Mary, D. Z. Renko, E. Gras, C. Thal. *Bioorg. Med. Chem. Lett.* **10**, 637 (2000).
- [48] D. M. Wong, H. M. Greenblatt, H. Dvir, P. R. Carlier, Y. F. Han, Y. P. Pang, I. Silman, J. L. Sussman. *J. Am. Chem. Soc.* **125**, 363 (2003).
- [49] H. Haviv, D. M. Wong, I. Silman, J. L. Sussman. *Curr. Top. Med. Chem.* **7**, 375 (2007).
- [50] M. Schulze, O. Siol, M. Decker, J. Lehmann. *Bioorg. Med. Chem. Lett.* **20**, 2946 (2010).
- [51] R. Otto, R. Penzis, F. Gaube, O. Adolph, K. J. Fohr, P. Warncke, D. Robaa, D. Appenroth, C. Fleck, C. Enzensperger, J. Lehmann, T. Winckler. *J. Med. Chem.* **58**, 6710 (2015).
- [52] S. Bachurin, E. Bukatina, N. Lermontova, S. Tkachenko, A. Afanasiev, V. Grigoriev, I. Grigorieva, Y. U. Ivanov, S. Sablin, N. Zefirov. *Ann. N. Y. Acad. Sci.* **939**, 425 (2001).
- [53] A. Ustyugov, E. Shevtsova, S. Bachurin. *Mol. Neurobiol.* **52**, 970 (2015).
- [54] R. S. Doody, S. I. Gavrilova, M. Sano, R. G. Thomas, P. S. Aisen, S. O. Bachurin, L. Seely, D. Hung. *Lancet* **372**, 207 (2008).
- [55] P. R. Bhargava, K. A. Bates, T. Porter, E. Teimouri, G. Perry, J. W. Steele, S. Gandy, D. Groth, R. N. Martins, G. Verdile. *Transl. Psychiatry* **3**, e332 (2013).
- [56] G. F. Makhaeva, E. F. Shevtsova, N. P. Boltneva, N. V. Kovaleva, E. V. Rudakova, L. G. Dubova, P. N. Shevtsov, S. O. Bachurin. *Dokl. Biochem. Biophys.* **484**, 1 (2019).
- [57] V. B. Sokolov, A. Y. Aksinenko, T. A. Epishina, T. V. Goreva. *Russ. J. Gen. Chem.* **88**, 1931 (2018).
- [58] V. B. Sokolov, A. Y. Aksinenko, T. V. Goreva, T. A. Epishina, A. N. Samsonova. *Russ. J. Gen. Chem.* **88**, 1266 (2018).
- [59] S. C. Laizure, V. Herring, Z. Hu, K. Witbrodt, R. B. Parker. *Pharmacotherapy* **33**, 210 (2013).
- [60] L. Di. *Curr Drug Metab* **20**, 91 (2019).
- [61] L. G. Tsurkan, M. J. Hatfield, C. C. Edwards, J. L. Hyatt, P. M. Potter. *Chem. Biol. Interact.* **203**, 226 (2013).
- [62] G. F. Makhaeva, E. V. Radchenko, I. I. Baskin, V. A. Palyulin, R. J. Richardson, N. S. Zefirov. *SAR QSAR Environ. Res.* **23**, 627 (2012).
- [63] G. F. Makhaeva, E. V. Radchenko, V. A. Palyulin, E. V. Rudakova, A. Y. Aksinenko, V. B. Sokolov, N. S. Zefirov, R. J. Richardson. *Chem. Biol. Interact.* **203**, 231 (2013).
- [64] G. F. Makhaeva, E. V. Rudakova, O. G. Serebryakova, A. Y. Aksinenko, S. V. Lushchekina, S. O. Bachurin, R. J. Richardson. *Chem. Biol. Interact.* **259(Pt B)**, 332 (2016).
- [65] G. F. Makhaeva, N. P. Boltneva, S. V. Lushchekina, O. G. Serebryakova, T. S. Stupina, A. A. Terentiev, I. V. Serkov, A. N. Proshin, S. O. Bachurin, R. J. Richardson. *Bioorg. Med. Chem.* **24**, 1050 (2016).
- [66] G. F. Makhaeva, E. V. Rudakova, N. V. Kovaleva, S. V. Lushchekina, N. P. Boltneva, A. N. Proshin, E. V. Shchegolkov, Y. V. Burgart, V. I. Saloutin. *Russ. Chem. Bull.* **68**, 967 (2019).

- [67] P. Taylor, S. Lappi. *Biochemistry* **14**, 1989 (1975).
- [68] S. V. Lushchekina, G. F. Makhaeva, D. A. Novichkova, I. V. Zueva, N. V. Kovaleva, R. J. Richardson. *Supercomput. Front. Innov.* **5**, 89 (2018).
- [69] R. Re, N. Pellegrini, A. Proteggente, A. Pannala, M. Yang, C. Rice-Evans. *Free Radic. Biol. Med.* **26**, 1231 (1999).
- [70] G. F. Makhaeva, V. B. Sokolov, E. F. Shevtsova, N. V. Kovaleva, S. V. Lushchekina, N. P. Boltneva, E. V. Rudakova, A. Y. Aksinenko, P. N. Shevtsov, M. E. Neganova, L. G. Dubova, S. O. Bachurin. *Pure Appl. Chem.* **89**, 1167 (2017).
- [71] P. R. Angelova, D. Vinogradova, M. E. Neganova, T. P. Serkova, V. V. Sokolov, S. O. Bachurin, E. F. Shevtsova, A. Y. Abramov. *Mol. Neurobiol.* **56**, 2244 (2019).
- [72] C. J. Cattanach, A. Cohen, B. Heath-Brown. *J Chem Soc Perkin* **1** **10**, 1235 (1968).
- [73] J. Poldy, R. Peakall, R. A. Barrow. *Tetrahedron Lett.* **49**, 2446 (2008).
- [74] G. L. Ellman, K. D. Courtney, V. Andres, R. M. Featherstone. *Biochem. Pharmacol.* **7**, 88 (1961).
- [75] S. H. Sterri, B. A. Johnsen, F. Fonnum. *Biochem. Pharmacol.* **34**, 2779 (1985).
- [76] P. Taylor, J. Lwebuga-Mukasa, S. Lappi, J. Rademacher. *Mol. Pharmacol.* **10**, 703 (1974).
- [77] A. G. Gonall, C. J. Bardawill, M. M. David. *J. Biol. Chem.* **177**, 751 (1949).
- [78] E. R. Milaeva, O. A. Gerasimova, Z. Jingwei, D. B. Shpakovsky, S. A. Syrbu, A. S. Semeykin, O. I. Koifman, E. G. Kireeva, E. F. Shevtsova, S. O. Bachurin, N. S. Zefirov. *J. Inorg. Biochem.* **102**, 1348 (2008).
- [79] K. E. O. Åkerman, M. K. F. Wikström. *FEBS Lett.* **68**, 191 (1976).
- [80] M. W. Schmidt, K. K. Baldridge, J. A. Boatz, S. T. Elbert, M. S. Gordon, J. H. Jensen, S. Koseki, N. Matsunaga, K. A. Nguyen, S. J. Su, T. L. Windus, M. Dupuis, J. A. Montgomery. *J. Comput. Chem.* **14**, 1347 (1993).
- [81] R. S. Mulliken. *J. Chem. Phys.* **23**, 1833 (1955).
- [82] J. Cheung, M. J. Rudolph, F. Burshteyn, M. S. Cassidy, E. N. Gary, J. Love, M. C. Franklin, J. J. Height. *J. Med. Chem.* **55**, 10282 (2012).
- [83] G. M. Morris, D. S. Goodsell, R. S. Halliday, R. Huey, W. E. Hart, R. K. Belew, A. J. Olson. *J. Comput. Chem.* **19**, 1639 (1998).
- [84] G. M. Morris, R. Huey, W. Lindstrom, M. F. Sanner, R. K. Belew, D. S. Goodsell, A. J. Olson. *J. Comput. Chem.* **30**, 2785 (2009).
- [85] E. V. Radchenko, A. S. Dyabina, V. A. Palyulin, N. S. Zefirov. *Russ. Chem. Bull., Intern. Ed.* **65**, 576 (2016).
- [86] A. S. Dyabina, E. V. Radchenko, V. A. Palyulin, N. S. Zefirov. *Dokl. Biochem. Biophys.* **470**, 371 (2016).
- [87] E. V. Radchenko, Y. A. Rulev, A. Y. Safanyayev, V. A. Palyulin, N. S. Zefirov. *Dokl. Biochem. Biophys.* **473**, 128 (2017).
- [88] ADMET prediction service. <http://qsar.chem.msu.ru/admet/> Accessed 01 Jul 2019.
- [89] I. Sushko, S. Novotarskyi, R. Korner, A. K. Pandey, M. Rupp, W. Teetz, S. Brandmaier, A. Abdelaziz, V. V. Prokopenko, V. Y. Tanchuk, R. Todeschini, A. Varnek, G. Marcou, P. Ertl, V. Potemkin, M. Grishina, J. Gasteiger, C. Schwab, I. I. Baskin, V. A. Palyulin, E. V. Radchenko, W. J. Welsh, V. Kholodovych, D. Chekmarev, A. Cherkasov, J. Aires-de-Sousa, Q. Y. Zhang, A. Bender, F. Nigsch, L. Patiny, A. Williams, V. Tkachenko, I. V. Tetko. *J. Comput. Aided Mol. Des.* **25**, 533 (2011).
- [90] G. R. Bickerton, G. V. Paolini, J. Besnard, S. Muresan, A. L. Hopkins. *Nat. Chem.* **4**, 90 (2012).
- [91] RDKit: open-source cheminformatics software. <http://www.rdkit.org>. Retrieved Aug 1, 2019.
- [92] V. Voevodin, A. Antonov, D. Nikitenko, P. Shvets, S. Sobolev, I. Sidorov, K. Stefanov, V. Voevodin, S. Zhumatiy. *Supercomput. Front. Innov.* **6**, 4 (2019).